

# Phase-Space Approach to Wannier Pairing and Bogoliubov Orbitals in Square-Octagon Lattices

Rajesh O. Sharma, and Tanmoy Das\*

Department of Physics, Indian Institute of Science, Bangalore 560012, India

\* [tnmydas@iisc.ac.in](mailto:tnmydas@iisc.ac.in)

## Abstract

Low-energy lattice models are the cornerstone for understanding many-body effects and interactions between systems and measurements. A key challenge lies in identifying appropriate states that canonically transform between momentum and real space while retaining the correlation, entanglement, and geometric properties — generally called the Wannier obstruction. Here, we introduce a phase-space approach to bypass these obstructions. Instead of treating phase space as a manifold, we embed real space through a Bloch vector space at each momentum. Orbital and spin states are introduced through product states with the Bloch vector, while quantum statistics, correlations, topology, and entanglements are inherited from the Hamiltonian. We apply this framework to explore unconventional pairing symmetry and the Bogoliubov-de-Gennes (BdG) equation in the phase space. Our findings demonstrate that while superconductivity exhibits global coherence in momentum space, the local Wannier orbital symmetry primarily determines the pairing symmetry. By engineering a flat band with artificial gauge fields, we analytically solve the spin-fluctuation mediated pairing symmetry on the phase space. We then apply the model to a square-octagon superconductor  $\text{Lu}_2\text{Fe}_3\text{Si}_5$  using density functional theory (DFT) to unravel a coexistence of nodeless  $s^\pm$  and nodal  $s_{z^2}$  pairing symmetries. This phase-space framework provides a robust, obstruction-free lattice model for complex many-body systems and their exotic excitations.

## Contents

<b>1</b>	<b>Introduction</b>	<b>2</b>
<b>2</b>	<b>The Phase Space Model</b>	<b>3</b>
2.1	Single particle Wannier fields	4
2.2	Many body Wannier fields and Density Matrix	5
2.3	Operators in the phase space	7
2.4	Density-density interaction and RPA	8
2.5	Mean fields in the phase space	9
2.6	Fermion parity	10
2.7	Wannier pairing and Bogoliubov Orbitals	10
2.8	Self-consistent SC gap equation	12
<b>3</b>	<b>Results and Discussions</b>	<b>13</b>
3.1	Single (flat) band superconductivity: Analytical solution	13
3.2	Bogoliubov orbitals	17

---

3.3	Tight-binding model and numerical solution	17
3.4	First-principles calculations	18
4	Conclusions	20
A	Density-Density interaction and Random Phase Approximation (RPA)	21
B	Example for Implementation of Fermion Parity	23
C	First-principles electronic structure calculations	24
	References	25

---

## 1 Introduction

Constructing low-energy lattice model to understand complex physical systems is a major challenge. Tight-binding models and Wannier orbital constructions, despite certain obstructions, work well for weakly correlated quasiparticles. [1–9]. But they face significant difficulties in intermediate or strongly correlated systems. [10–14] In such cases, long-wavelength field theories near critical points are often used, though they are prone to ultraviolet and infrared divergences. A lattice theory, which is free from these obstructions and divergences, would be invaluable to describe exotic excitations in many-body ground states — such as magnetic order, spin liquids, fractional quantum Hall or superconducting (SC) states — and for evaluating the matrix-element effects of the system-measurement couplings.

For a lattice model of quasiparticle excitations, there must exist  $N$  linearly independent Wannier states in real space, corresponding to  $N$  Bloch states in momentum space, connected by a Fourier transformation. However, even for non-interacting quasiparticles, topology or degeneracy can obstruct this transformation. [4, 6–9, 15, 16] For exotic excitations, additional challenges arise to obtain canonical transformation between position and momentum space for properties such as quantum statistics, fractional quantum numbers, correlations, and geometric properties. [5, 17–23].

The conventional variational method works by constructing a many-body ground state to serve as the vacuum state for low-energy excitations defined in either real or momentum space. Here, we extend this approach to the position-momentum *phase space*. Rather than treating phase space as a manifold, we embed position space into a Bloch vector space at each momentum (or vice versa) and construct a variational wavefunction as a product of a Bloch vector and orbital-like excitations. Quantum statistics, correlations, and geometric properties are introduced via projection operators, while non-local unitary transformations generate entanglement between particle-hole pairs, spin-orbit/spin-momentum locking, and/or topology. Operators, Hamiltonians, order parameters, and mean-field theories are represented in phase space, while expectation values are transformed into momentum or real space as desired.

We apply this phase-space framework to study mean-field superconductivity and spin-fluctuation-mediated unconventional pairing symmetries. Spin-fluctuation theory and pairing eigenvalues are derived in phase space, allowing us to solve the pairing problem analytically. Our results show that while superconductivity exhibits global coherence in momentum space, local lattice symmetry constrained Wannier orbital dictates the pairing symmetry. Additionally, we also find that the Bogoliubov-de-Gennes (BdG) Hamiltonian and the corresponding

Bogoliubov transformation become non-local (local) in real (momentum) space. This enables us to localize particle-hole entangled Bogoliubov states in real space, reflecting further the symmetry correspondence between the Wannier orbitals and pairing symmetry.

As a case study, we examine a square-octagon (SO) lattice. In the first case, we study a flat band scenario in a tight-binding model with artificial gauge fields. Wannier orbitals and pairing states are constructed in phase space, enabling analytical solutions for pairing symmetry. We recast the BdG equation in the phase space by expanding both the SC gap and the dispersions terms in the same irreducible representation of the Bloch vector space. This gives insights into how the Wannier orbitals and pairing symmetry conspire in real space to manifest a global coherence in the superconducting (SC) ground state. The method also allows us to obtain local Bogoliubov excitations of the SC condensate.

Next, we consider a recently discovered superconductor in SO material  $\text{Lu}_2\text{Fe}_3\text{Si}_5$  within the DFT calculation, followed by the Wannier orbital calculation.  $\text{Lu}_2\text{Fe}_3\text{Si}_5$  exhibits characteristics of a two-band superconductor with  $T_c \sim 6.1$  K. The specific heat measurements [24–28] and penetration depth experiments [29, 30] indicate the presence of nodeless pairing symmetry, leaving open questions about whether the pairing mechanism is conventional (attractive) or unconventional (repulsive). On the other hand, the rapid suppression of  $T_c$  caused by non-magnetic impurities [31–34], and atomic disorder induced by neutron irradiation [35], suggests that  $\text{Lu}_2\text{Fe}_3\text{Si}_5$  is an unconventional superconductor exhibiting superconductivity [36].

Using DFT-derived Wannier orbitals, we solve the spin-fluctuation-mediated pairing eigenvalue equation for  $\text{Lu}_2\text{Fe}_3\text{Si}_5$ . The material’s strong three-dimensionality stabilizes compact Wannier orbitals with  $s_{z^2}$  and  $d_{z^2}$  wave symmetries. Dominant spin fluctuations arise in both inter- and intraband channels, mediating a coexistence of an unconventional nodeless, isotropic  $s^\pm$ -wave pairing and a nodal  $s_{z^2}$  channel. This  $s+s$  pairing symmetry is in agreement with the temperature dependence of the magnetic penetration depth measurements, which is well-described by an  $s+s$  pairing channel [29].

The rest of the paper is arranged as follows. We devote Sec. 2 to develop the full formalism of phase-space orbital theory. We present the single particle state in Sec. 2.1 many-body state in Sec. 2.2 and phase space operators Sec. 2.3. In Sec. 2.4, we discuss the random-phase-approximation (RPA) to evaluate spin and charge fluctuation mediated pairing interaction. We follow it by the construction of the mean fields, the inclusion of quantum statistics, the orbital constructions of Bogoliubov orbitals, and the self-consistent pairing gap equation in the following four subsections. We present the result of a tight-binding model and flat band superconductivity in Sec. 3.1. We consider the pairing symmetry calculations starting from the DFT result for  $\text{Lu}_2\text{Fe}_3\text{Si}_5$  in Sec. 3.4. Finally, we conclude in Sec. 4.

## 2 The Phase Space Model

Let us start with  $\mathbf{r}$  and  $\mathbf{k}$  being continuous position and momentum variables spanning the entire system. We calibrate  $\mathbf{r}$  with respect to the unit cell (UC) as  $\mathbf{r} = \mathbf{r} + \mathbf{R}$ , where  $\mathbf{R} \in \mathbb{Z}_{L^d}$  are the positions of the UCs and  $\mathbf{r} \in \text{UC}$  is the position within a UC.  $L^d$  is the total number of UCs in a  $d$ -dimensional lattice (lattice constant  $\mathbf{a} = \mathbf{1}$ ) with a periodic boundary condition:  $L + \mathbf{1} \sim \mathbf{1}$  (see Fig. 1). Similarly, we split the momentum space as  $\mathbf{k} = \mathbf{k} + \mathbf{G}$ , where  $\mathbf{k} \in \mathbb{T}^d$  lies in a  $d$ -dimensional torus, and  $\mathbf{G}$  is the reciprocal lattice vector. The finite lattice of  $L^d$  sites discretizes the Brillouin zone (BZ)  $\mathbb{T}^d$  with a grid size of  $\Delta\mathbf{k} = 2\pi/L$ , such that  $\mathbf{k} \in \mathbb{Z}_{L^d}$ . This makes the  $\mathbf{k}$  space a Pontryagin dual of the  $\mathbf{R}$  space. The Fourier transformation between the two spaces is obtained by a polynomial of degree  $L_d$  with the basis function of  $\mathbf{z}_{\mathbf{R}}(\mathbf{k}) = e^{i\mathbf{k}\cdot\mathbf{R}}$ . In fact, if we associate Hilbert spaces of  $\mathcal{L}^2(\mathbb{T}^d)$  and  $\mathcal{L}^2(\mathbb{Z}_{L^d})$  in the corresponding momentum and position spaces, respectively, then  $\mathbf{z}_{\mathbf{R}}(\mathbf{k})$  serves as the component of

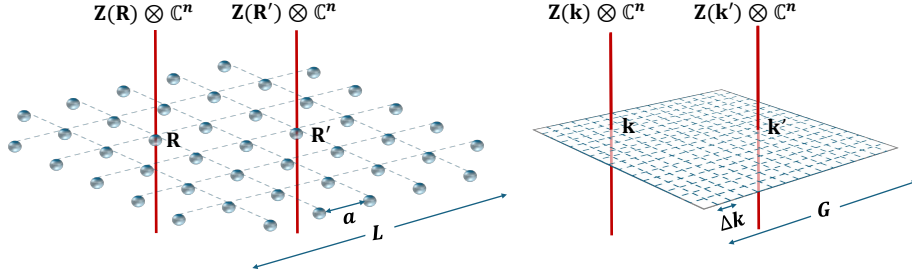


Figure 1: The real-space lattice of length  $L = Na$  is split into unit cell of length  $a$ . Correspondingly, Similarly, the BZ is split with a grid size of  $\Delta\mathbf{k} = 2\pi/L$  and repeated by the reciprocal lattice vector  $\mathbf{G} = 2\pi/a$ . At each lattice site  $\mathbf{R}$ , we introduce a product state of the Bloch phase vector  $\mathbf{Z}(\mathbf{R})$  and Wannier orbital spinor  $\mathbb{C}^n$ , where  $n = n \times s$  for  $n$  bands and  $s$  spins. We introduce a product state  $\mathbf{Z}(\mathbf{k}) \otimes \mathbb{C}^n$  at each  $\mathbf{k}$  point. Note that the Wannier orbitals  $\mathbb{C}^n$  are assumed to have a maximum uncertainty within a unit cell in real space maximum uncertainty of  $\Delta\mathbf{k}$  within a BZ. We consider a trivial bundle where the same orbitals are included at all  $\mathbf{k}$  and  $\mathbf{R}$  points, where additional gauge obstruction, correlation and entanglement arise from the Hamiltonian.

a unitary transformation between them. This gives us the idea to construct a linearly independent Bloch basis vector at each  $\mathbf{k}$  from each column of  $\mathbf{z}_{\mathbf{R}}(\mathbf{k})$ . We denote the basis vector at each  $\mathbf{k}$  as  $\mathbf{Z}(\mathbf{k}) := 1/\sqrt{L^d} (z_1(\mathbf{k}) \dots z_{L^d}(\mathbf{k}))^T$ . The same dimensional vector space  $\mathbf{Z}(\mathbf{R})$  is also defined at each  $\mathbf{R}$  from the rows of  $\mathbf{z}_{\mathbf{R}}(\mathbf{k})$ .

Therefore,  $\mathbf{Z}(\mathbf{k}) \in \mathcal{L}^2(\mathbb{T}^d)$  can be considered as sections of a vector bundle  $\mathbb{E}_{\mathbf{k}} \rightarrow \mathbb{T}^d$  (where  $\mathbb{E}_{\mathbf{k}}$  is the total space). Similarly,  $\mathbf{Z}(\mathbf{R}) \in \mathcal{L}^2(\mathbb{Z}_{L^d})$  is a section of the real space vector bundle  $\mathbb{E}_{\mathbf{R}} \rightarrow \mathbb{Z}_{L^d}$ . Note that we have not made any assumption about the orientability of the bundles, and a bundle-isomorphism (Fourier transformation) exists between them. Next, we introduce a Hilbert space  $\mathbb{C}^{(n \times s)}$  for the internal degrees of freedom  $n, s$  for band (Wannier orbital) and spin indices at each base point  $\mathbf{k}$  and  $\mathbf{R}$  of their respective manifolds. Without losing generality, we start with a trivial vector bundle by considering a tensor product state as  $\mathcal{H}_{\mathbf{k}/\mathbf{R}} := \mathbf{Z}(\mathbf{k}/\mathbf{R}) \otimes \mathbb{C}^{(n \times s)}$ . The existence of Wannier orbitals for the Bloch eigenstates states is encoded in the existence of the bundle-isomorphism between them. This trivialization of the vector bundle in the momentum (and real) space does not exclude the Wannierization of the topological insulators and certain flat band systems.

We now discuss how to express fields and operators in the above representations. Let  $f(\mathbf{r})$  be a local field in real space. It can be defined in the periodic lattice as  $\int d\mathbf{r} f(\mathbf{r}) = \sum_{\mathbf{R}} \int_{\text{UC}} d\mathbf{r} f_{\mathbf{R}}(\mathbf{r})$ , where  $f_{\mathbf{R}}(\mathbf{r}) = f(\mathbf{r} - \mathbf{R})$ . We can define a vector field  $\mathbf{f}(\mathbf{r}) = (f_1(\mathbf{r}) f_2(\mathbf{r}) \dots)^T$ , such that its projection on the periodic plane wave basis becomes

$$f(\mathbf{k}, \mathbf{r}) = \mathbf{Z}^\dagger(\mathbf{k}) \mathbf{f}(\mathbf{r}) = \sum_{\mathbf{R}} \mathbf{z}_{\mathbf{R}}^*(\mathbf{k}) f_{\mathbf{R}}(\mathbf{r}), \quad (1)$$

$\forall \mathbf{r} \in \text{UC}, \forall \mathbf{k} \in \text{BZ}$ . We use this protocol to define the fields and operators in the phase space.

## 2.1 Single particle Wannier fields

Suppose we are interested in constructing Wannier states of the  $2N$  ( $2$  for spins) bands across the Fermi level. These states are obtained by the projector  $\mathcal{P}(\mathbf{k}) = \sum_n |\mathbf{k}, n\rangle \langle \mathbf{k}, n|$ , where

$|\mathbf{k}, \mathbf{n}\rangle$  are the corresponding eigenstates of the full Hamiltonian.  $\mathbf{n} = (\mathbf{n}, s)$  is assumed to be a composite index for band ( $\mathbf{n} = 1, \dots, N$ ) and spin ( $s = \uparrow, \downarrow$ ). According to the prescription outline above, we start with a tensor product basis  $|\mathbf{k}, \mathbf{n}\rangle = |\mathbf{k}\rangle \otimes |\mathbf{n}\rangle \otimes |s\rangle \in \mathcal{H}_{\mathbf{k}}$ .

Next, we project the single-particle states to the real space  $|\mathbf{r}_n, \mathbf{n}\rangle$ , where  $\mathbf{r}_n$  is the position of the  $n^{\text{th}}$  Wannier orbital. We write  $\mathbf{r}_n = \mathbf{r}_n - \mathbf{R}$ , where  $\mathbf{r}_n \in$  unit cell are the Wyckoff positions of the  $n^{\text{th}}$ -Wannier orbital. Then we expand  $|\mathbf{R}, \mathbf{n}, s_z\rangle \in \mathcal{H}_{\mathbf{R}}$  on the basis of  $|\mathbf{k}, \mathbf{n}, s\rangle$ , and define the expansion coefficients as  $e^{i\mathbf{k}\cdot\mathbf{r}}\Psi_{\mathbf{R}ns}(\mathbf{k}, \mathbf{r})$ , where  $\Psi_{\mathbf{R}ns}(\mathbf{k}, \mathbf{r})$  is a product of three spinors:

$$\Psi_{\mathbf{R}ns}(\mathbf{k}, \mathbf{r}) = z_{\mathbf{R}}(\mathbf{k})w_n(\mathbf{r})\chi_s. \quad (2)$$

Here,  $z_{\mathbf{R}}(\mathbf{k}) = \langle \mathbf{R} | \mathbf{k} \rangle$  are the plane waves of the periodic part,  $w_n(\mathbf{r}) = \langle \mathbf{r}_n | \mathbf{n} \rangle$  are the Wannier state with spins  $\chi_s = \langle s_z | s \rangle$ . All the states are assumed to form complete bases in their usual way. (We drop the index  $\mathbf{n}$  in  $\mathbf{r}$  associated with  $w_n$  for simplicity and insert it back in the cases when the meaning is obscured.)<sup>1</sup>

The spinors for the orbital and spin space are defined as  $\mathbf{W} = 1/\sqrt{N}(w_1 \ w_2 \ \dots \ w_N)^T \forall \mathbf{r}$ , and  $\mathbf{X} = 1/\sqrt{2}(\chi_{\uparrow} \ \chi_{\downarrow})^T$ . The spinor for the Bloch phases can be arranged in various ways. It is convenient to split the  $L$ -dimensional vector as  $\mathbf{Z}(\mathbf{k}) = \mathbf{Z}_1(\mathbf{k}) \oplus \mathbf{Z}_2(\mathbf{k}) \oplus \dots$ , where  $\mathbf{Z}_\alpha(\mathbf{k}) := 1/\sqrt{d_\alpha}(z_{\mathbf{R}_1}(\mathbf{k}) \ \dots \ z_{\mathbf{R}_{d_\alpha}}(\mathbf{k}))^T$  is the vector for the  $\alpha^{\text{th}}$  nearest neighbor with  $d_\alpha$  number of sites. For short-range interaction, the Bloch spinor can be truncated up to a few nearest neighbors.

Therefore, we have a single particle spinor defined at each  $(\mathbf{k}, \mathbf{r})$  as

$$\Psi(\mathbf{k}, \mathbf{r}) = \mathbf{Z}(\mathbf{k}) \otimes \mathbf{W}(\mathbf{r}) \otimes \mathbf{X}. \quad (3)$$

In the Wannier spinor  $\mathbf{W}(\mathbf{r})$ ,  $\mathbf{r}$  is assumed to be the set of Wyckoff positions of all the Wannier orbitals within an UC. Although this is a good starting point for a single particle state, if we not do not have any information of the many-body ground state. However, unitary rotations can further be employed depending on the Hamiltonian's details and symmetry (see Appendix B.<sup>2</sup>

## 2.2 Many body Wannier fields and Density Matrix

As mentioned in the introduction, a many-body ground state can be viewed as the vacuum for low-energy excitations. When the nature of these excitations is unknown, the statistical phase can be treated as a variational parameter. Notably, there are three primary sources of correlations: quantum statistics, Hamiltonian-induced interactions, and geometric effects. In what follows, without loss of generality, we can start with a product state of individual excitations as the many-body ground state and incorporate all three correlations as variational parameters. Building on this idea, we construct a two-body Wannier state in phase space. The

<sup>1</sup>The wavefunction, in its present form, is localized at  $\mathbf{k}$  with a maximum uncertainty given by the BZ grid size of  $\Delta\mathbf{k}_x \sim (2\pi/L)$ , and at  $\mathbf{r}$  with a maximum uncertainty within a unit cell of lattice constant  $\Delta\mathbf{x} \sim \mathbf{a}$  ( $\mathbf{a}$  is the lattice constant), along the  $\mathbf{x}$ -direction. This appears to violate the uncertain relation  $\Delta\mathbf{p}\Delta\mathbf{x} \sim 2\pi\hbar(\mathbf{a}/L)$ . But we know that the  $\Psi_{\mathbf{R}ns}(\mathbf{k}, \mathbf{r})$  are periodic functions in the lattice, and hence are defined modulo  $\mathbf{R}$  which makes  $\Delta\mathbf{x} \sim L$  and the uncertainty relation is saturated. Other possible states include wavepacket state which can be implemented by modifying  $z_{\mathbf{R}}(\mathbf{k})$  from its plane wave solution to, say, a Gaussian state.

<sup>2</sup>For example, owing to a given site-symmetry group of the Wannier functions, one can rotate to the irreps basis of the Wannier states by suitable unitary rotation to  $\mathbf{W}(\mathbf{r})$  [37, 38]. Similarly, sometimes it's easier to work in the angular momentum basis for the Bloch phase  $\mathbf{Z}(\mathbf{k})$ , as discussed in Appendix B. Furthermore, due to atomic (or Rashba-type) spin-orbit coupling, the orbital (or momentum) and spin states are entangled, and one needs to go to the total angular momentum (or helicity) basis for the single-particle basis by calculating the Clebsch-Gordon coefficients. In both cases, it is easy to implement any symmetry of the theory, say  $\mathbf{g}$ , as  $\mathcal{U}_{\mathbf{g}} = U_{\mathbf{g},z} \otimes U_{\mathbf{g},w} \otimes U_{\mathbf{g},x}$ , where  $U_{\mathbf{g},z}$  is the  $\mathcal{N} \times \mathcal{N}$  unitary (or anti-unitary) representation of the symmetry  $\mathbf{g}$  in the  $\mathbf{Z}$  spinor, and so on. The single particle state transforms as  $\Psi(\mathbf{k}, \mathbf{r}) \rightarrow \mathcal{U}_{\mathbf{g}}\Psi(\mathbf{g}\mathbf{k}, \mathbf{g}\mathbf{r}) = (U_{\mathbf{g},z}\mathbf{Z}(\mathbf{g}\mathbf{k})) \otimes (U_{\mathbf{g},w}\mathbf{W}(\mathbf{g}\mathbf{r})) \otimes (U_{\mathbf{g},x}\mathbf{X})$ .

wavefunction can then be partitioned into the two-body Bloch phase, orbital, and spin sectors as follows:

$$\begin{aligned}\Psi^{(2)}(\mathbf{k}_{1,2}, \mathbf{r}_{1,2}) &= P_\theta [\Psi(\mathbf{k}_1, \mathbf{r}_1) \otimes \Psi(\mathbf{k}_2, \mathbf{r}_2)], \\ &= \mathcal{Z}(\mathbf{k}_{1,2}) \otimes \mathcal{W}(\mathbf{r}_{1,2}) \otimes \mathcal{X}.\end{aligned}\quad (4)$$

Here we have partitioned the pair density fields in the three channels with individual fermion parity, as  $\mathcal{Z}(\mathbf{k}_{1,2})=P_{\theta(Z)} [\mathcal{Z}(\mathbf{k}_1) \otimes \mathcal{Z}(\mathbf{k}_2)]$ ,  $\mathcal{W}(\mathbf{r}_{1,2})=P_{\theta(W)} [\mathcal{W}(\mathbf{r}_1) \otimes \mathcal{W}(\mathbf{r}_2)]$ , and  $\mathcal{X}=P_{\theta(X)} [\mathcal{X} \otimes \mathcal{X}]$ . The components of these pair fields are

$$\begin{aligned}\mathcal{Z}_{R_{1,2}}(\mathbf{k}_{1,2}) &= P_{\theta(R_{12})}[z_{R_1}(\mathbf{k}_1)z_{R_2}(\mathbf{k}_2)], \\ \mathcal{W}_{n_{1,2}}(\mathbf{r}_{1,2}) &= P_{\theta(n_{12})}[w_{n_1}(\mathbf{r}_1)w_{n_2}(\mathbf{r}_2)], \\ \mathcal{X}_{s_{1,2}} &= P_{\theta(s_{1,2})}[\chi_{s_1}\chi_{s_2}].\end{aligned}\quad (5)$$

$P_{\theta=\pi}$  is the fermion exchange parity such that the total wavefunction is an eigenstate of the fermion exchange parity operator with the eigenvalues of  $e^{i\pi}$ . The fermion parity operator is split among its quantum numbers as  $P = P_{\theta(Z)} \otimes P_{\theta(W)} \otimes P_{\theta(X)}$ . Now, we make an interesting observation that the individual product state, say,  $\mathcal{Z} \otimes \mathcal{Z}$ , is an eigenstate of the corresponding parity  $P_{\theta(Z)}$  operator, but its eigenvalue is *not* required to be  $e^{i\pi}$ . The same argument applies to  $P_{\theta(W)}$  and  $P_{\theta(X)}$  operators,. However, the total phase must satisfy  $\theta(\mathcal{Z}) + \theta(\mathcal{W}) + \theta(\mathcal{X}) = \pi$ .<sup>3</sup> The projection  $P_\theta$  onto the two-particle states introduces a quantum correlation between the excitations.

An interaction term in the Hamiltonian introduces correlation between the particles, which can be included via a projection operator  $e^{\mathbf{J}_{R_{12}}(\mathbf{k}_{1,2}, \mathbf{r}_{1,2})}$  where  $\mathbf{J}$  is a rank-(1,1) Jastrow factor tensor. The specific form of  $\mathbf{J}$  is Hamiltonian dependent.

Finally, we discuss the correlation property arising from geometric effects. A low-energy theory serves as an effective description confined to a specific subspace of the full Hilbert space (e.g. a few bands near the Fermi level, a flat band, the lowest Landau level in the fractional quantum Hall (FQH) state, or singlet pair for superconductivity or a spin liquid phase.) To ensure completeness and orthogonality for the orbitals defined in a subspace, we invoke a projection operator  $\mathcal{P}(\mathbf{k}) = \sum_{\mathbf{n}} |\mathbf{n}, \mathbf{k}\rangle \langle \mathbf{n}, \mathbf{k}| \neq \mathbb{I}$  to the low-energy subspace of  $\mathbf{n}$  states of our interest. This projection introduces correlations (or, equivalently, imposes constraints on the correlation function), which we call geometry-induced correlations. [40]

In a way, a projection operator is similar to a reduced-density matrix. A density matrix field or transfer matrix in the phase space can be defined as

$$\rho(\mathbf{k}_{1,2}, \mathbf{r}_{1,2}) = \Psi(\mathbf{k}_2, \mathbf{r}_2) \otimes \Psi^\dagger(\mathbf{k}_1, \mathbf{r}_1) = \mathcal{Z}(\mathbf{k}_{1,2}) \otimes \mathcal{W}(\mathbf{r}_{1,2}) \otimes \mathcal{X}.\quad (6)$$

The components of the three density fields are

$$\begin{aligned}\mathcal{Z}_{R_{1,2}}(\mathbf{k}_{1,2}) &= z_{R_1}^*(\mathbf{k}_1)z_{R_2}(\mathbf{k}_2), \\ \mathcal{W}_{n_{1,2}}(\mathbf{r}_{1,2}) &= w_{n_1}^*(\mathbf{r}_1)w_{n_2}(\mathbf{r}_2), \\ \mathcal{X}_{s_{1,2}} &= \chi_{s_1}^*\chi_{s_2}.\end{aligned}\quad (7)$$

<sup>3</sup>Since each quantum number does not necessarily have to be the eigenvalue of their fermion parities, even and odd parity mixings lead to exotic superconducting (or many-body) states. For example, in non-unitary superconductors, such mixing between singlet and triplet governs novel phase transition [39]. Furthermore, the Bloch phase factors can have geometric phases such as the Ahronov-Bohm phase or Berry phase on non-trivial topological geometry, which makes the SC states more interesting. Similarly generalization of Eq. (4) to anyonic cases will be easier. One can, in principle, treat  $\theta$  as a variational parameter for exotic many-body systems such as for fractional quantum Hall state or in flat band Chern insulators where anyon, Majorana or parafermion excitations are expected.

For any index  $\mathbf{a}$ , we define a composite index  $\mathbf{a}_{1,2} = (\mathbf{a}_1, \mathbf{a}_2)$ .  $\mathbf{R}_1 = \mathbf{R}_2$  gives the local density while  $\mathbf{R}_1 \neq \mathbf{R}_2$  giving a transfer matrix between different unit cells. Owing to translation invariance, the density matrix depends on the relative wavevector  $\mathbf{q} = \mathbf{k}_1 - \mathbf{k}_2$  - called the density wave ordering vector.

### 2.3 Operators in the phase space

We now discuss the one-body operator  $T(\mathbf{r})$ , and two-body operator  $V(\mathbf{r}_{1,2})$  in the phase space representations in Eqs. (3), and (4). We do it in two steps for a better illustration. First, we obtain the tensor components of these operators in the Bloch phases. Next, we obtain the matrix elements of each tensor component for the orbital and spin states.

Proceeding as in Eq. (1), we obtain the tensor components of a one-body operator  $\mathbf{T}(\mathbf{r})$  in the Bloch phase basis as

$$T(\mathbf{k}, \mathbf{r}) = Z^\dagger(\mathbf{k})T(\mathbf{r})Z(\mathbf{k}) = \sum_{\mathbf{R}_{1,2}} T_{\mathbf{R}_{1,2}}(\mathbf{r})Z_{\mathbf{R}_{1,2}}(\mathbf{k}), \quad (8)$$

where  $T_{\mathbf{R}_{1,2}}(\mathbf{r})$  is a (1,1)-tensor at  $\mathbf{r}$ . We identify this as the tight-binding hopping tensor between the sites  $\mathbf{R}_{1,2}$ . We have implemented the translational invariance, which makes  $\mathbf{k}$  to be the same for the coming and departing states. Similarly, the two-body operator  $V(\mathbf{r}_{1,2})$  is written as

$$\begin{aligned} V(\mathbf{k}_{1-4}, \mathbf{r}_{1,2}) &= Z^\dagger(\mathbf{k}_{1,2})V(\mathbf{r}_{1,2})Z(\mathbf{k}_{3,4})\delta_{\mathbf{k}_{1-4}}, \\ &= \sum_{\mathbf{R}_{1-4}} \bar{V}_{\mathbf{R}_{1,3}}^{\mathbf{R}_{2,4}}(\mathbf{r}_{1,2})Z_{\mathbf{R}_{1,2}}^*(\mathbf{k}_{1,2})Z_{\mathbf{R}_{3,4}}(\mathbf{k}_{3,4})\delta_{\mathbf{k}_{1-4}}. \end{aligned} \quad (9)$$

$\delta_{\mathbf{k}_{1-4}} = \delta(\mathbf{k}_1 + \mathbf{k}_2 - \mathbf{k}_3 - \mathbf{k}_4)$  implements momentum conservation due to the translational invariance. The operator  $\bar{V} = P_{\theta(\mathbf{R}_{1,2})}VP_{\theta(\mathbf{R}_{3,4})}^{-1}$  is a (2,2)-tensor at each value of  $\mathbf{r}, \mathbf{r}'$ , which is projected onto the fermionic odd parity sector (as illustrated in Eq. (13) below).

Next, we evaluate the matrix elements of each tensor component on the Wannier orbital and spin basis. For the single particle Hamiltonian, we obtain

$$\begin{aligned} H_T &= \int_{\mathbf{k}, \mathbf{r}} \Psi^\dagger(\mathbf{k}, \mathbf{r})T(\mathbf{r})\Psi(\mathbf{k}, \mathbf{r}) |\mathbf{k}\rangle \langle \mathbf{k}| \\ &= \int_{\mathbf{k}, \mathbf{r}} \sum_{n_{1,2}} T(\mathbf{k}, \mathbf{r})\mathcal{W}_{n_{1,2}}(\mathbf{r})\mathcal{X}_{s_{1,2}}|n_1, \mathbf{k}\rangle \langle n_2, \mathbf{k}|, \\ &= \int_{\mathbf{k}} \sum_{n_{1,2}} T_{n_{1,2}}(\mathbf{k})|n_1, \mathbf{k}\rangle \langle n_2, \mathbf{k}|. \end{aligned} \quad (10)$$

Here  $\int_{\mathbf{k}, \mathbf{r}} \equiv \int_{\mathbf{k}} \int_{\mathbf{r}} \equiv \sum_{\mathbf{k} \in \text{BZ}} \int_{\mathbf{r} \in \text{UC}} d\mathbf{r}$  is the integration over the phase space volume where  $\mathbf{k} \in \text{BZ}$  and  $\mathbf{r} \in \text{UC}$  integrations are assumed to be normalized with their corresponding BZ and UC volumes, respectively. Note that the other phase factor  $e^{i\mathbf{k}\cdot\mathbf{r}}$  drops out here. Recall that the composite index  $n_i = (n_i, s_i)$  combines Wannier orbital and spin indices. We define  $T_{\mathbf{R}_{1,2}, n_{1,2}} = \int_{\mathbf{r}} T_{\mathbf{R}_{1,2}, n_{1,2}}(\mathbf{r})\mathcal{W}_{n_{1,2}}(\mathbf{r})\mathcal{X}_{s_{1,2}}$  as tight-binding hopping tensor and  $T_{n_{1,2}}(\mathbf{k}) = \sum_{\mathbf{R}_{1,2}} T_{\mathbf{R}_{1,2}, n_{1,2}}Z_{\mathbf{R}_{1,2}}(\mathbf{k})$  is the corresponding dispersion.

Similarly, the two-particle Hamiltonian reads:

$$\begin{aligned} H_V &= \int_{\mathbf{k}_{1-4}, \mathbf{r}_{1,2}} \Psi^{(2)\dagger}(\mathbf{k}_{1,2}, \mathbf{r}_{1,2})V(\mathbf{r}_{1,2})\Psi^{(2)}(\mathbf{k}_{3,4}, \mathbf{r}_{1,2})\delta_{\mathbf{k}_{1-4}}(\mathbf{r}_{1,2}) |\mathbf{k}_{1,2}\rangle \langle \mathbf{k}_{3,4}|, \\ &= \int_{\mathbf{k}_{1-4}} \sum_{n_{1-4}} \bar{V}_{n_{1,3}}^{n_{2,4}}(\mathbf{k}_{1-4})|n_{1,2}, \mathbf{k}_{1,2}\rangle \langle n_{3,4}, \mathbf{k}_{3,4}|. \end{aligned} \quad (11)$$

Here, the Wannier interaction vertex is defined as

$$\begin{aligned}\bar{V}_{n_{1,3}}^{n_{2,4}}(\mathbf{k}_{1-4}), &= \int_{\mathbf{r}_{1,2}} \bar{V}_{n_{1,3}}^{n_{2,4}}(\mathbf{k}_{1-4}, \mathbf{r}_{1,2}) \delta_{\mathbf{k}_{1-4}}(\mathbf{r}_{1,2}) \mathbb{W}_{n_{1,2}}^*(\mathbf{r}_{1,2}) \mathbb{W}_{n_{3,4}}(\mathbf{r}_{1,2}) \mathbb{X}_{s_{1,2}}^* \mathbb{X}_{s_{3,4}}, \\ &= \sum_{\mathbf{R}_{1-4}} \bar{V}_{\mathbf{R}_{1,3}, n_{1,3}}^{\mathbf{R}_{2,4}, n_{2,4}} \mathbb{Z}_{\mathbf{R}_{1,2}}^*(\mathbf{k}_{1,2}) \mathbb{Z}_{\mathbf{R}_{3,4}}(\mathbf{k}_{3,4}) \delta_{\mathbf{k}_{1-4}}\end{aligned}\quad (12)$$

where  $\delta_{\mathbf{k}_{1-4}}(\mathbf{r}_{1,2}) = \delta_{\mathbf{k}_{1-4}} \exp(i \sum_{a=1}^4 \mathbf{k}_a \cdot \mathbf{r}_a)$ , with  $\mathbf{r}_a$  being the center of the  $a^{\text{th}}$  Wannier orbital. In the chosen product basis, we can split the Wannier interaction as  $\bar{V}_{\mathbf{R}_{1,3}, n_{1,3}}^{\mathbf{R}_{2,4}, n_{2,4}} = \mathbb{P}_\theta \left[ V_{\mathbf{R}_{1,3}}^{\mathbf{R}_{2,4}} \otimes V_{n_{1,3}}^{n_{2,4}} \otimes V_{s_{1,3}}^{s_{2,4}} \right] \mathbb{P}_\theta^{-1}$ . We will, henceforth, omit the bar symbol from the two-body terms for simplicity in notion, and all such two-body terms are assumed to be antisymmetric under the fermionic exchange. It is worthwhile noting that Eq. (12) can also be expressed in terms of the density matrices (Eq. (7) as shown in Eq. (38)), however, it easier to implement the exchange parity symmetry in terms of the pair fields.

By invoking translational invariance, we set  $\mathbf{R}_3 = \mathbf{R}_4 = \mathbf{0}$  for the initial states. In addition, we often consider onsite interactions, i.e.  $\mathbf{R}_1 = \mathbf{R}_2 = \mathbf{0}$ . This means  $V_{\mathbf{R}_{1,3}}^{\mathbf{R}_{2,4}} = \mathbb{I} \delta_{\mathbf{R}_{1-4}, \mathbf{0}}$ . (The corresponding  $\mathbf{R}_{1,2} \neq \mathbf{0}$  components give the so-called extended Hubbard model, which we ignore here.) We can write the remaining orbital and spin parts in the eigenbasis of exchange parity as:

$$V_{\theta(W)} = \frac{1}{2} \left( V_{n_{1,3}}^{n_{2,4}} + e^{i\theta(W)} V_{n_{2,4}}^{n_{1,3}} \right), \quad V_{\theta(X)} = \frac{1}{2} \left( V_{s_{1,3}}^{s_{2,4}} + e^{i\theta(X)} V_{s_{2,4}}^{s_{1,3}} \right). \quad (13)$$

Typically, for the fermion case of present interest, in the absence of any gauge fields, we have  $\theta = \mathbf{0}, \pi$  as  $\mathbb{P}_\theta^2 = \mathbb{1}$ . Then we have two allowed choices: orbital symmetric, spin antisymmetric:  $V_{W+} V_{X-}$ , and orbital antisymmetric and spin symmetric:  $V_{W-} V_{X+}$  parts. We identify these interactions in terms of known interactions in Sec. 2.4 and Appendix A. For systems with spin-orbit coupling and other entanglement properties, we implement the unitary rotation (*c.f.* Chebsch-Gordon coefficients) in the interaction term.

## 2.4 Density-density interaction and RPA

A common origin of interactions in materials is density-density interactions. As mentioned in Sec. 2.3, we only consider ‘onsite’ interactions, i.e., the Bloch basis part gives  $V_{\mathbf{R}_{1,3}}^{\mathbf{R}_{2,4}} = \mathbb{I} \delta_{\mathbf{R}_{1-4}, \mathbf{0}}$ . For the orbital part, we have two sources of interaction, namely the orbital density-density  $V_{nn}^{mm} = V_{n_{1,3}}^{n_{2,4}} \delta_{n_{1,3}} \delta_{n_{2,4}}$ , and the orbital exchange part, also known as pair hopping interaction,  $V_{nm}^{nm}$ . Similarly, for spins, we have spin density-density interaction  $V_{ss}^{tt}$ , and spin-flip term  $V_{st}^{st}$ . Their combined interactions that follow the fermion parity are recognized in the literature as follows:

$$V_{nn}^{nn} V_{ss}^{\bar{s}\bar{s}} = U_n, \quad V_{nn}^{mm} V_{ss}^{tt} = U'_{mn}, \quad V_{nn}^{mm} V_{st}^{st} = J_{mn}, \quad V_{nm}^{nm} V_{ss}^{\bar{s}\bar{s}} = J'_{mn}. \quad (14)$$

Here, we assume  $m \neq n$ , while both  $s = t$  and  $s \neq t$  are allowed.  $\bar{s} = -s$ . The interactions are often spin-independent unless spin-orbit coupling is included. Here  $U$ , and  $U'$  are the intra- and inter-Wannier orbitals Hubbard interactions, respectively, while  $J$  and  $J'$  are Hund’s coupling and pair hopping terms. The corresponding interacting Hamiltonian is called the Hubbard-Kanamori Hamiltonian [41–43].

Such onsite repulsive interaction is often inapt to give unconventional (momentum dependent) pairing state. However, the many-body effects, such as spin and charge fluctuation, can



produce short-range interactions between the nearest Wannier states, which can be attractive between Cooper pairs of opposite phases. The lowest order renormalization of the density-density interaction arises from the random-phase approximation (RPA) for intermediate to weak coupling theory [12, 44–50]. We derive the RPA-dressed interaction  $\Gamma$  in Appendix A, and quote the result here:

$$\begin{aligned} \Gamma_{R_{13}, n_{13}}^{R_{24}, n_{24}}(\mathbf{q}) &= V_{n_{13}}^{n_{24}} + \frac{3}{2} \sum_{n_{5678}, s_{56}} V_{n_{15}}^{n_{26}}(\Pi_s)_{R_{13}, n_{57}, s_{55}}^{R_{24}, n_{68}, s_{66}}(\mathbf{q}) V_{n_{73}, s_{53}}^{n_{84}, s_{64}} \\ &\quad - \frac{1}{2} \sum_{n_{5678}, s_{56}} V_{n_{15}}^{n_{26}}(\Pi_c)_{R_{13}, n_{57}, s_{55}}^{R_{24}, n_{68}, s_{66}} V_{n_{73}, s_{53}}^{n_{84}, s_{64}}(\mathbf{q}). \end{aligned} \quad (15)$$

$\mathbf{q}$  gives the momentum transfer between the initial and final states. In the above, we have occasionally expanded the compact index  $\mathbf{n} = (\mathbf{n}, \mathbf{s})$  when we have substituted the same or different spin states. For example, in the third (fourth) term, we have substituted  $s_7 = \mp s_5$ , and  $s_8 = \mp s_6$ . The first term is the onsite interaction, the second term corresponds to the spin-flip ( $\uparrow\downarrow \leftrightarrow \downarrow\uparrow$ ) fluctuation – called the transverse spin fluctuation, and the third term corresponds to occupation density or charge fluctuation.  $\Pi_{s/c}$  refers to the RPA susceptibility, which is related to the Lindhard susceptibility  $\Pi$  as  $\Pi_{s/c} = \Pi(\mathbf{I} \mp \mathbf{V}\Pi)^{-1}$  where  $\mathbf{I}$  is the unit matrix. The  $A$  symbol denotes that we have written the rank-(2,2) tensor  $A$  in a matrix form (sometimes called a superoperator). The details are given in Appendix A.

## 2.5 Mean fields in the phase space

Here we introduce the mean-field decomposition of the interaction term in Eq. (12), except we replace the bare interaction ( $V$ ) with the RPA interaction  $\Gamma$ . To do that, we expand the RPA interaction in the phase space in the Wannier basis as

$$\Gamma_{R_{13}, n_{13}}^{R_{24}, n_{24}}(\mathbf{q}) = \int_{\mathbf{r}_{12}} \Gamma_{R_{13}, n_{13}}^{R_{24}, n_{24}}(\mathbf{r}_{12}) Z_{R_{12}}^*(\mathbf{q}) Z_{R_{34}}(-\mathbf{q}) W_{n_{1,2}}^*(\mathbf{r}_{1,2}) W_{n_{3,4}}(\mathbf{r}_{1,2}) X_{s_{1,2}}^* X_{s_{3,4}}. \quad (16)$$

Here  $W$  and  $X$  are to be read quasiparticle/excitation states which interact via the RPA interaction. By substituting  $\mathbf{q} = \mathbf{k}_1 - \mathbf{k}_2$  and integrating over  $(\mathbf{k}_2, \mathbf{r}_2)$  variables, we can define two local field tensors at  $(\mathbf{k}_1, \mathbf{r}_1)$ , namely the density field ( $\Omega$ ) and the pairing field  $\Delta$  as

$$\Omega_{R_{1,3}, n_{1,3}}(\mathbf{k}_1, \mathbf{r}_1) = \int_{\mathbf{k}_2, \mathbf{r}_2} \sum_{R_{2,4}, n_{2,4}} \Gamma_{R_{1,3}, n_{1,3}}^{R_{2,4}, n_{2,4}}(\mathbf{r}_{1,2}) Z_{R_{2,4}}(\mathbf{k}_{1,2}) W_{n_{2,4}}(\mathbf{r}_2) X_{s_{2,4}}. \quad (17)$$

(Similarly, an exchange field would be defined as  $\Omega_{R_{1,4}, n_{1,4}}(\mathbf{k}_1, \mathbf{r}_1)$ .) Finally, we define a mean-field one-body pairing tensor field as

$$\Delta_{R_{1,2}, n_{1,2}}(\mathbf{k}_1, \mathbf{r}_1) = \int_{\mathbf{k}_2, \mathbf{r}_2} \sum_{R_{3,4}, n_{3,4}} \Gamma_{R_{1,3}, n_{1,3}}^{R_{2,4}, n_{2,4}}(\mathbf{r}_{1,2}) Z_{R_{3,4}}(\mathbf{k}_{1,2}) W_{n_{3,4}}(\mathbf{r}_2) X_{s_{3,4}}. \quad (18)$$

$\Delta$  is antisymmetrized over the pair fields integrated out. In the reminder, we only consider the SC order parameter  $\Delta$ , and the procedure follows similarly for density wave orders  $\Omega$ . Once we substitute the pair field in Eq. (11), we obtain a single-particle (mean-field) Hamiltonian,

which can be written, in analogy with Eq. (8) as

$$\begin{aligned}
H_\Delta &= \int_{\mathbf{k}, \mathbf{r}} \sum_{\mathbf{R}_{1,2}, \mathbf{n}_{1,2}} \Delta_{\mathbf{R}_{1,2}, \mathbf{n}_{1,2}}(\mathbf{k}, \mathbf{r}) \mathbb{W}_{\mathbf{n}_{1,2}}^*(\mathbf{r}) \mathbb{X}_{s_{1,2}}^* | \mathbf{R}_{1,2} \mathbf{n}_{1,2} \mathbf{k} \rangle \\
&= \int_{\mathbf{k}} \sum_{\mathbf{R}_{1,2}, \mathbf{n}_{1,2}} \Delta_{\mathbf{R}_{1,2}, \mathbf{n}_{1,2}} \mathbb{Z}_{\mathbf{R}_{1,2}}^*(\mathbf{k}) | \mathbf{R}_{1,2} \mathbf{n}_{1,2} \mathbf{k} \rangle \\
&= \int_{\mathbf{k}} \sum_{\mathbf{n}_{12}} \Delta_{\mathbf{n}_{12}}(\mathbf{k}) | \mathbf{n}_{1,2} \mathbf{k} \rangle.
\end{aligned} \tag{19}$$

Here we call  $\Delta_{\mathbf{R}_{1,2}, \mathbf{n}_{1,2}} = \int_{\mathbf{r}} \Delta_{\mathbf{R}_{1,2}, \mathbf{n}_{1,2}}(\mathbf{r}) \mathbb{W}_{\mathbf{n}_{1,2}}^*(\mathbf{r}) \mathbb{X}_{s_{1,2}}^*$  as the ‘Wannier pairing field’ tensor between the Wannier sites  $\mathbf{R}_1, \mathbf{R}_2$  and orbitals  $\mathbf{n}_1$  and  $\mathbf{n}_2$ . And the pairing term in the momentum space is obtained as  $\Delta_{\mathbf{n}_{1,2}}(\mathbf{k}) = \sum_{\mathbf{R}_{1,2}} \Delta_{\mathbf{R}_{1,2}, \mathbf{n}_{1,2}} \mathbb{Z}_{\mathbf{R}_{1,2}}^*(\mathbf{k})$ . The pair field tensor is antisymmetric under the fermion parity.

The above procedure can be repeated for the mean-field density wave order parameter localized on the Wannier basis. We do not pursue this exercise in this work.

## 2.6 Fermion parity

The implementation of the fermion parity is an important distinction of the pairing field  $\Delta$  compared to the density wave field. Without losing generality, we can continue to implement the parity in the product basis for the three quantum numbers and move to any entangled or irreps basis with appropriate unitary transformations after incorporating the fermion parity. [51–53] In the total state, we can also arrange the even and odd parity states as

$$\begin{aligned}
\mathbb{Z} \otimes \mathbb{W} \otimes \mathbb{X} &\xrightarrow{U_{\theta(z)} \otimes U_{\theta(w)} \otimes U_{\theta(x)}} \begin{pmatrix} \mathbb{Z}_+ \\ \mathbb{Z}_- \end{pmatrix} \otimes \begin{pmatrix} \mathbb{W}_+ \\ \mathbb{W}_- \end{pmatrix} \otimes \begin{pmatrix} \mathbb{X}_+ \\ \mathbb{X}_- \end{pmatrix} \\
&\rightarrow \begin{pmatrix} \mathbb{Z}_+ \otimes \mathbb{W}_+ \otimes \mathbb{X}_- \\ \mathbb{Z}_+ \otimes \mathbb{W}_- \otimes \mathbb{X}_+ \\ \mathbb{Z}_- \otimes \mathbb{W}_+ \otimes \mathbb{X}_+ \\ \mathbb{Z}_- \otimes \mathbb{W}_- \otimes \mathbb{X}_- \end{pmatrix} \oplus (\text{even parity}).
\end{aligned} \tag{20}$$

On the right-hand side, we have rearranged the odd and even parity states for presentation purposes. One introduces a projection operator  $P_\theta$  to eliminate the even parity state. These are the four odd parity states allowed for superconductivity [53–57]. By substituting Eq. (20) in Eq. (18) we obtain the mean-field expression for the SC gap functions in the product basis of orbital, spin, and Bloch phase. In what follows, we can now switch from each pair of indices  $(\mathbf{R}_{1,2}, \mathbf{n}_{1,2}, s_{1,2})$  to their even/odd parity indices  $(\nu_{\mathbf{R}}, \nu_n, \nu_s)$  where  $\nu_i = \pm$  runs over the even and odd combinations of the index under the constraint at the total parity is odd  $\nu = -1$ .

## 2.7 Wannier pairing and Bogoliubov Orbitals

The nature of excitations depends on the Bell or Cooper pair fields condensed in the ground state. By breaking such pairs, one obtains two entangled or fractional excitations. They are often defined by a superposition state of the two quasiparticles that formed the pair state. [58]

For the Cooper pair case, such excitations are called the Bogoliubov quasiparticles, which are expressed in the Wannier basis by doubling the single particle spinors for particles and hole states:

$$\begin{aligned}
\Phi(\mathbf{k}, \mathbf{r}) &= [\Psi(\mathbf{k}, \mathbf{r}) \oplus \Psi^*(-\mathbf{k}, \mathbf{r})] \\
&= [\mathbb{Z}(\mathbf{k}) \otimes \mathbb{W}(\mathbf{r}) \otimes \mathbb{X}] \oplus [\mathbb{Z}(-\mathbf{k}) \otimes \mathbb{W}^*(\mathbf{r}) \otimes \mathbb{X}^*].
\end{aligned} \tag{21}$$

Here, we have already implemented a zero center-of-mass momentum for the Cooper pair by setting  $-\mathbf{k}$  for the second electron. “\*” stands for complex conjugation, which gives the hole states at  $\mathbf{k}$  for corresponding particle state at  $\mathbf{k}$ , and vice versa. In what follows, we can separate the particle-hole entanglement in the total states among the spatial, orbital, and spin parts, such that localization of the Bogoliubov quasiparticles is warranted.

We express a (mean-field) one-body BdG Hamiltonian in the particle-hole spinor as

$$\begin{aligned} H &= \int_{\mathbf{k}, \mathbf{r}} \Phi^\dagger(\mathbf{k}, \mathbf{r}) (T(\mathbf{r}) + \Delta(\mathbf{r})) \Phi(\mathbf{k}, \mathbf{r}), \\ &= \int_{\mathbf{k}} \sum_{\mathbf{R}_{1,2}, \mathbf{n}_{1,2}} \left[ T_{\mathbf{R}_{1,2}, \mathbf{n}_{1,2}} \mathcal{Z}_{\mathbf{R}_{1,2}}(\mathbf{k}) |\mathbf{R}_1 \mathbf{n}_1 \mathbf{k}\rangle \langle \mathbf{R}_2 \mathbf{n}_2 \mathbf{k}| \right. \\ &\quad \left. + \Delta_{\mathbf{R}_{1,2}, \mathbf{n}_{1,2}} \mathcal{Z}_{\mathbf{R}_{1,2}}(\mathbf{k}) |\mathbf{R}_1 \mathbf{n}_1 \mathbf{k}\rangle \langle \mathbf{R}_2 \mathbf{n}_2 - \mathbf{k}| \right] \end{aligned} \quad (22)$$

Note that the Bloch phase parts for the density and pairing part (with  $\mathbf{k} = -\mathbf{k}$ ) follow the identity  $\mathcal{Z}_{\mathbf{R}_{1,2}}(\mathbf{k}) = \mathcal{Z}_{\mathbf{R}_{2,1}}(-\mathbf{k}) = \mathcal{Z}_{\mathbf{R}_{1,2}}(\mathbf{k}) = \mathcal{Z}_{\mathbf{R}_{2,1}}(-\mathbf{k}) = z_{\mathbf{R}_1}(\mathbf{k}) z_{\mathbf{R}_2}^*(\mathbf{k})$  if we set  $\mathbf{R}_1 = \mathbf{0}$  due to translational symmetry. Therefore, the Bloch phase part can be taken as common from the above two terms, and we can define a (non-local) BdG Hamiltonian between the Wannier sites  $\mathbf{R}_1$  and  $\mathbf{R}_2$  at each  $\mathbf{k}$  as [59]

$$H_{\mathbf{R}_{1,2}} = \begin{pmatrix} T_{\mathbf{R}_{1,2}} & \Delta_{\mathbf{R}_{1,2}} \\ \Delta_{\mathbf{R}_{1,2}}^\dagger & -T_{\mathbf{R}_{1,2}}^T \end{pmatrix}, \quad (23)$$

where  $T$  and  $\Delta$  are rank-(1-1) tensors (indexed by  $\mathbf{R}_{1,2}$ ) with each component being a matrix in the orbital and spin space (index by  $\mathbf{n}_{1,2}$ ). The Hermitian conjugate and transpose operations are defined in the orbital and spin basis.  $H$  follows the particle-hole symmetry as

$$C_{\mathbf{R}_2} H_{\mathbf{R}_{1,2}} C_{\mathbf{R}_1}^{-1} = -H_{\mathbf{R}_{2,1}}, \quad C_{\mathbf{R}} = \begin{pmatrix} \mathbf{0} & \mathbb{I} \\ \mathbb{I} & \mathbf{0} \end{pmatrix} \mathcal{K}, \quad (24)$$

where  $\mathcal{K}$  is the complex conjugation and  $C_{\mathbf{R}}$  is a local particle-hole operator defined in the orbital and spin basis at  $\mathbf{R}$ .

We diagonalize the Hamiltonian in two steps. First, we employ a (local) similarity transformation  $\mathcal{S}_{\mathbf{R}}$  that diagonalizes the orbital and spin parts of  $T$ . Note that  $\mathcal{S}_{\mathbf{R}}$  is a local rank-1 tensor which is a unitary matrix in the orbital and spin basis, and follows a ‘unitarity’ condition between the Wannier sites as

$$\sum_{\mathbf{R}_{1,2}} \mathcal{S}_{\mathbf{R}_1}^\dagger \mathcal{S}_{\mathbf{R}_2} \mathcal{Z}_{\mathbf{R}_{1,2}}(\mathbf{k}_{1,2}) = \mathbb{I} \delta_{\mathbf{k}_{1,2}}. \quad (25)$$

This gives the hopping and the pairing interaction in the band basis (denoted by  $\alpha$ ) as

$$\begin{aligned} T_{\mathbf{R}_{1,2}, \alpha_1} \delta_{\alpha_1, 2} &= \sum_{\mathbf{n}_{1,2}} \mathcal{S}_{\mathbf{R}_1, \mathbf{n}_1, \alpha_1} T_{\mathbf{R}_{1,2}, \mathbf{n}_{1,2}} \mathcal{S}_{\mathbf{R}_2, \mathbf{n}_2, \alpha_2}^\dagger, \\ \Delta_{\mathbf{R}_{1,2}, \alpha_1, 2} &= \sum_{\mathbf{n}_{1,2}} \mathcal{S}_{\mathbf{R}_1, \mathbf{n}_1, \alpha_1} \Delta_{\mathbf{R}_{1,2}, \mathbf{n}_{1,2}} \mathcal{S}_{\mathbf{R}_2, \mathbf{n}_2, \alpha_2}. \end{aligned} \quad (26)$$

(We have kept the same notation  $T$  and  $\Delta$  in both orbital and band basis for simplicity in notation.)  $\alpha_i$  index denotes the band basis, in which the orbital and spin can be mixed if there is a spin-orbit coupling term. Since  $T$  and  $\Delta$  do not necessarily commute,  $\Delta$  is not necessarily diagonal in the band basis. This local transformation faces gauge obstruction if the band structure

or the pairing state is topologically non-trivial, where an additional parallel transport/Wilson line is to be included between the  $\mathbf{R}_{1,2}$  sites with a flux conservation constraint [40].

Next, we diagonalize the BdG Hamiltonian in Eq. (22) by the Bogoliubov transformation as defined by the unitarity matrix at each tensor component  $\mathbf{R}$ :

$$U_{\mathbf{R}} = \begin{pmatrix} \mathcal{U}_{\mathbf{R}} & -\mathcal{V}_{\mathbf{R}} \\ \mathcal{V}_{\mathbf{R}}^{\dagger} & \mathcal{U}_{\mathbf{R}}^{\dagger} \end{pmatrix}. \quad (27)$$

$\mathcal{U}$  and  $\mathcal{V}$  are also rank-1 tensors in the Bloch phase basis, with each component being a matrix on the band basis. The non-local Bogoliubov transformation is defined as  $U_{\mathbf{R}_2} \mathcal{S}_{\mathbf{R}_2} H_{\mathbf{R}_{1,2}} \mathcal{S}_{\mathbf{R}_1}^{\dagger} U_{\mathbf{R}_1}^{\dagger} = -D_{\mathbf{R}_{1,2}}$  where  $D_{\mathbf{R}_{1,2}}$  is a diagonal matrix consistent of the Bogoliubov quasiparticle energies. The ‘unitarity’ condition of  $U_{\mathbf{R}}$ , as for  $\mathcal{S}_{\mathbf{R}}$  in Eq. (25), yields

$$\begin{aligned} \sum_{\mathbf{R}_{1,2}} (\mathcal{U}_{\mathbf{R}_1}^{\dagger} \mathcal{U}_{\mathbf{R}_2} + \mathcal{V}_{\mathbf{R}_1}^{\dagger} \mathcal{V}_{\mathbf{R}_2}) \mathcal{Z}_{\mathbf{R}_{1,2}}(\mathbf{k}_{1,2}) &= \mathbb{I} \delta_{\mathbf{k}_{1,2}}, \\ \sum_{\mathbf{R}_{1,2}} (\mathcal{U}_{\mathbf{R}_1} \mathcal{V}_{\mathbf{R}_2}^{\dagger} - \mathcal{U}_{\mathbf{R}_2} \mathcal{V}_{\mathbf{R}_1}^{\dagger}) \mathcal{Z}_{\mathbf{R}_{1,2}}(\mathbf{k}_{1,2}) &= \mathbf{0}. \end{aligned} \quad (28)$$

It is worthwhile pointing out the momentum space representation of these quantities: The band dispersion and the gap function can be retrieved in the momentum space as usual by  $\xi_{\alpha_1}(\mathbf{k}) = \sum_{\mathbf{R}_{1,2}} t_{\mathbf{R}_{1,2},\alpha_1} \mathcal{Z}_{\mathbf{R}_{1,2}}(\mathbf{k})$ ,  $\Delta_{\alpha_{1,2}}(\mathbf{k}) = \sum_{\mathbf{R}_{1,2}} \Delta_{\mathbf{R}_{1,2},\alpha_{1,2}} \mathcal{Z}_{\mathbf{R}_{1,2}}(\mathbf{k})$ ,  $\mathcal{S}(\mathbf{k}) = \sum_{\mathbf{R}} \mathcal{S}_{\mathbf{R}} z_{\mathbf{R}}(\mathbf{k})$ , and the same for  $U(\mathbf{k})$ . The fermion parity in the orbital basis is preserved in the band basis.

We can similarly define the Wannier orbitals of the Bogoliubov quasiparticles, namely the Bogoliubov orbitals. We define the Bogoliubov spinor as

$$\mathbf{B}(\mathbf{r}) \oplus \mathbf{B}^*(\mathbf{r}) = [\mathcal{U} \mathcal{S}(\mathbf{W}(\mathbf{r}) \otimes \mathbf{X})] \oplus [-\mathcal{V} \mathcal{S}^*(\mathbf{W}^*(\mathbf{r}) \otimes \mathbf{X}^*)]. \quad (29)$$

Since the unitary transformations mix the orbital and spins, there is no general way to disentangle them in the Bogoliubov quasiparticle basis.  $\mathbf{B}(\mathbf{r})$  is a spinor of the Wannier orbitals of the Bogoliubov quasiparticles. However, one can proceed similarly to define Fourier components of the Bogoliubov orbitals in phase space as  $\mathbf{B}(\mathbf{k}, \mathbf{r}) = \mathbf{Z}(\mathbf{k}) \otimes \mathbf{B}(\mathbf{r})$ . Since spin and orbitals are mixed in the Bogoliubov states, we do not separate the spin and orbital part here. Under certain conditions,  $\mathbf{B}(\mathbf{r})$  become Wannier spinor of Majorana orbitals. [17, 18, 40, 60] There may arise obstruction in gauge fixing in the Wannier orbitals of Bogoliubov (or general entangled) quasiparticles, which needs gauge fields to obtain orthonormalized orbitals states [40]. However, we do not pursue this endeavor in this paper.

## 2.8 Self-consistent SC gap equation

Our final step is to obtain the self-consistent gap equation in the band basis of  $\mathcal{S}\Psi$ . The RPA interaction vertex in the band basis reads

$$\Gamma_{\mathbf{R}_{1,3},\alpha_{1,3}}^{\mathbf{R}_{2,4},\alpha_{2,4}} = \sum_{n_{1,2,3,4}} \Gamma_{\mathbf{R}_{1,3},n_{1,3}}^{\mathbf{R}_{2,4},n_{2,4}} \mathcal{S}_{\mathbf{R}_1,n_1,\alpha_1}^{\dagger} \mathcal{S}_{\mathbf{R}_2,n_2,\alpha_2}^{\dagger} \mathcal{S}_{\mathbf{R}_3,n_3,\alpha_3} \mathcal{S}_{\mathbf{R}_4,n_4,\alpha_4}. \quad (30)$$

To obtain the self-consistent gap equation, we apply the  $\mathcal{S}_{\mathbf{R}}$  rotation on both sides of Eq. (18), Eq. (26), and (30). Finally, we apply the  $U_{\mathbf{R}}$  rotation. Following Eq. (13), and Eq. (20), the interaction  $\Gamma$  and gap function  $\Delta$  are decoupled in the even and odd fermion parity channels for the space, orbital, and spin parts. This gives the self-consistent gap equation as

$$\Delta_{\nu_{\mathbf{R}},\bar{\nu}_a} \mathcal{Z}_{\nu_{\mathbf{R}}}(\mathbf{k}_1) = \int_{\mathbf{k}_2} \sum_{\nu'_{\mathbf{R}},\nu'_a} \Gamma_{\nu_{\mathbf{R}},\bar{\nu}_a}^{\nu'_{\mathbf{R}},\nu'_a}(\mathbf{k}_{1,2}) \langle (\mathcal{U}\mathcal{V})_{\nu'_{\mathbf{R}},\bar{\nu}'_a} \mathcal{Z}_{\nu'_{\mathbf{R}}}(\mathbf{k}_2) \rangle_{\text{BCS}}. \quad (31)$$

We recall that the indices  $\nu_i = \pm$  stand for even and odd parity basis for each quantum number  $i$ . We denote  $\bar{\nu}_i$  as the opposite parity to  $\nu_i$ . For example, we denote  $\Delta_{\nu_R, \bar{\nu}_a}$  to imply that if it's even (odd) under the exchange between  $\mathbf{R}_{1,2}$ , it must be odd (even) in the band basis  $\alpha_{1,2}$  and vice versa. Note that although the Bloch basis seems to be separated from the orbital part in the above formalism, the odd parity constraint entangled all the indices. At temperature  $T \rightarrow 0$ , the expectation value on the wavefunction can be expanded in a Taylor series in terms of  $\Delta$ , and restricting ourselves to the linear term in  $\Delta$ , we define  $\langle (\mathcal{UV})_{\nu'_R, \bar{\nu}'_a} Z_{\nu'_R}(\mathbf{k}_2) \rangle_{\text{BCS}} \approx -\lambda^{-1} \Delta_{\nu'_R, \bar{\nu}'_a} Z_{\nu'_R}(\mathbf{k}_2) + \mathcal{O}((\Delta/T)^2)$ , where  $T$  represents bandwidth. Here  $\lambda$  is a SC coupling constant, and its dimension is [Energy]. A minus sign is chosen as we expect that a solution exists for attractive potential  $\Gamma$ . This converts Eq. (31) into an eigenvalue equation as

$$\int_{\mathbf{k}_2} \sum_{\nu'_R, \bar{\nu}'_n} \Gamma_{\nu'_R, \bar{\nu}'_n}^{\nu'_R, \bar{\nu}'_n}(\mathbf{k}_{1,2}) \Delta_{\nu'_R, \bar{\nu}'_n} Z_{\nu'_R}(\mathbf{k}_2) = -\lambda \Delta_{\nu_R, \bar{\nu}_n} Z_{\nu_R}(\mathbf{k}_1). \quad (32)$$

To solve the above eigenvalue equation, we construct a superoperator  $\Gamma$  and supervector  $|\Delta\rangle$  by vectorizing each pair of indices [61]. Typically, the SC gap function is short-ranged, and hence, we can truncate the Bloch phase basis up to, say,  $N_R$  nearest neighbors. We consider  $N_\alpha^F$  number of Fermi momenta (in  $d$  dimension) for the  $\alpha^{\text{th}}$  energy band. Then we have a total of  $N_F = \sum_\alpha N_\alpha^F$ . With  $S = 1/2$  spins, we have a  $N_{\text{tot}} = 2N_R N_F$  dimensional vector  $|\Delta\rangle$  and  $N_{\text{tot}} \times N_{\text{tot}}$  dimensional matrix  $\Gamma$ . We solve for the largest eigenvalue  $\lambda > 0$  of  $\Gamma$  and the corresponding eigenvector  $|\Delta\rangle$  gives the pairing symmetry of the theory. We express the eigenvector in the matrix form between different bands, spins, and Wannier sites, and this is the final result.

As a variational approach, we can first find the symmetry-allowed Bloch functions  $Z$  in the pair state and find expectation values of  $\Gamma$  in these basis states. Then, the highest negative value of this expectation value gives us the pairing symmetry.

## 3 Results and Discussions

### 3.1 Single (flat) band superconductivity: Analytical solution

To illustrate the formalism, we begin with a simple four-band tight-binding model on a 2D square octagon (SO) lattice, as shown in Fig. 2(a).<sup>4</sup> Previous tight-binding calculations for a spinless orbital per sublattices on the 2D SO lattice with four sublattices have shown four dispersive metallic bands [62–64]. Pal has shown that with a suitable insertion of magnetic flux through the diamond plaquette, as shown in Fig. 4(b), a topological flat band can be achieved. [62]

A lattice model with magnetic flux is studied by expanding the lattice to a magnetic unit cell that threads an done for U(1) flux in Ref. [65], and for  $Z_2$  flux in Ref. [40] Here, we focus on flux  $\Phi = \Phi_0$  per diamond plaquette (unit cell) is an integer. This choice makes the magnetic unit cell coincide with the flux-free unit cell. Finally, among the four bands, we focus on the spinless single flat band. The corresponding Wannier orbital is localized at the center of the diamond plaquette and gives a dual square lattice. Because there is no Peierls phase between the diamond plaquette, the hopping between the Wannier orbitals,  $T_{\mathbf{R}_{1,2}}$ , does not contain any complex phase. We, however, focus on the nearly flat bands such that a well-defined Fermi Surface (FS) contour is present to construct a superconductivity theory due to FS instability and solve it analytically.

<sup>4</sup>Note that we explored several monolayer SO materials using DFT calculations and so far found no stable lattice to report here. Thus, the 2D structure studied here serves purely as a theoretical example.

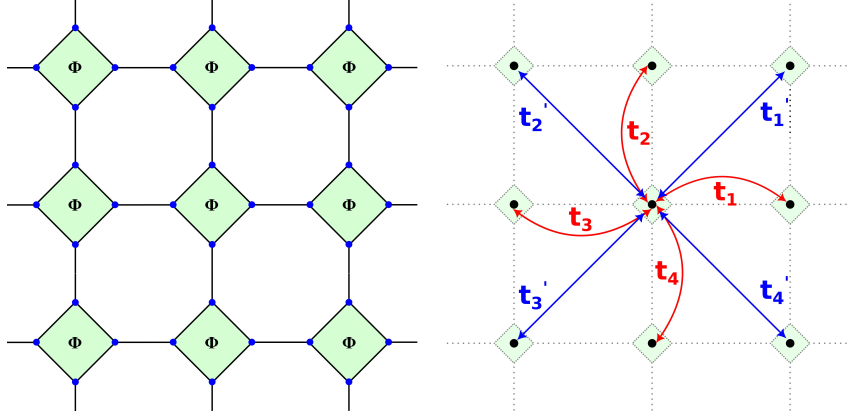


Figure 2: A 2D square octagon (SO) lattice with four sublattices forming a diamond plaquette (green shade). Following Ref. [62] we consider an integer flux threading each diamond plaquette, which produces a flat band (see Fig. 4). We consider a single Wannier orbital model for the flat-band, which is localized at the diamond center. We consider first (second) nearest neighbor hoppings  $t_i$  ( $t'_i$ ) between these orbitals to draw a phase diagram of pairing symmetry as summarized in Table 1.

In Eq. (22), the hopping matrix  $T_{\mathbf{R}_{12}}$  and the pairing  $\Delta_{\mathbf{R}_{12}}$  terms are expanded on the basis of  $\mathcal{Z}_{\mathbf{R}_{1,2}}(\mathbf{k})$  and  $\mathbb{Z}_{\mathbf{R}_{1,2}}(\mathbf{k})$ , respectively. Owing to translational symmetry, we set  $\mathbf{R}_1 = \mathbf{0}$ , reducing both these bases to  $\mathbf{z}_{\mathbf{R}_2}(\mathbf{k})$ , and the BdG Hamiltonian can be written as in Eq. (23). The fermion odd parity in  $\mathbf{z}_{\mathbf{R}}(\mathbf{k})$  (the subscript ‘2’ in  $\mathbf{R}_2$  is omitted) simply translates into parity under the operation of inversion (I) :  $\mathbf{k} \rightarrow -\mathbf{k}$ . Therefore, instead of the trivial plane wave basis  $\mathbf{z}_{\mathbf{R}}(\mathbf{k})$ , we transform them to the basis that satisfies  $\mathbf{z}_\nu(\mathbf{k}) = \pm \mathbf{z}_\nu(-\mathbf{k})$ . We transform the Bloch basis to the irreducible representations (irreps) of the point group symmetry and use the gauge freedom condition to choose the irreps basis that is even or odd under the parity.

We arrange the Bloch basis in the invariant subspace of the point-group symmetry as  $\mathbf{Z}(\mathbf{k}) = \mathbf{Z}_1(\mathbf{k}) \oplus \mathbf{Z}_2(\mathbf{k}) \oplus \dots$ . Here for the  $i^{\text{th}}$  - nearest neighbors with  $d_i$  number of sites, we define a  $d_i$ -dimensional vector as  $\mathbf{Z}_i := (z_1 \dots z_{d_i})^T$ ,  $\forall \mathbf{k}$ . For the 2D SO lattice belonging to the  $D_{4h}$  group, the irreducible representations (irreps) are  $A \otimes B \otimes E$ . We show that each nearest neighbor vector belongs to one of the irreps.

Table 1: The irreps from Eq. (33) are presented with corresponding  $\mathbf{k}$  space representation, parity and tight-binding hoppings and required FS topology to produce pairing states in a repulsing interaction scenario.  $t_{\mathbf{R}}$  ( $t'_{\mathbf{R}}$ ) are the nearest neighbor shopping elements from  $\mathbf{R} = \mathbf{0}$  to four of the  $\{\mathbf{R}\}_1$  ( $\{\mathbf{R}\}_2$ ) Wannier sites. The results are the same for  $\Delta_\nu$  in terms of nearest neighbors  $\Delta_{\mathbf{R}}$ .

Basis ( $\mathbf{z}_\nu$ )	$\mathbf{k}$ -rep	G irrep	Parity	$t_\nu$	FS for pairing
$\mathbf{z}_{s_x 2+y^2}$	$\cos k_x + \cos k_y$	$A_1$	+1	$(t_1 + t_2 + t_3 + t_4)/2$	No pairing
$\mathbf{z}_{d_x 2-y^2}$	$\cos k_x - \cos k_y$	$B_1$	+1	$(t_1 - t_2 + t_3 - t_4)/2$	All FS topologies
$\mathbf{z}_{p_x/p_y}$	$i\sqrt{2} \sin k_{x/y}$	$E$	-1	$\sqrt{2}(t_{1,2} - t_{3,4})$	Small (e-/h-) FSs
$\mathbf{z}_{s_x 2y^2}$	$2 \cos k_x \cos k_y$	$A_1$	+1	$(t'_1 + t'_2 + t'_3 + t'_4)/2$	Near half-filling
$\mathbf{z}_{d_{xy}}$	$2 \sin k_x \sin k_y$	$B_2$	+1	$(t'_1 - t'_2 + t'_3 - t'_4)/2$	For small (e-/h-) FSs
$\mathbf{z}_{p_{x\pm y}}$	$i\sqrt{2} \sin(k_x \pm k_y)$	$E$	-1	$\sqrt{2}(t'_{1,2} - t'_{3,4})$	For small (e-/h-) FSs

On a square lattice, we have  $d_i = 4 \forall i$ , as shown in Fig. 2. For the first nearest neighbor ( $i = 1$ ), we have  $\{\mathbf{R}\}_1 = (\pm 1, 0), (0, \pm 1)$ , for the second nearest neighbor ( $i = 2$ )

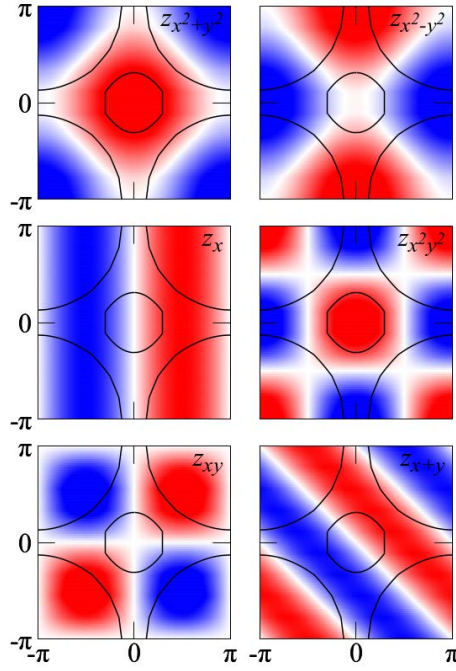


Figure 3: Plot of the pairing functions  $z_n$ . The red and blue regions represent the positive and negative values of the function, respectively. The lines show some schematic FS contours to demonstrate the pairing function changes sign on the corresponding FS. A small FS centering the  $\Gamma$  point corresponds to an electron-like FS, while a large FS centering the  $\mathbf{k} = (\pi, \pi)$  point corresponds to a slight hole doping.

$\{\mathbf{R}\}_2 = (\pm 1, \pm 1)$ , and so on. The invariant subspaces can be written in the irreps as

$$\begin{aligned}
 \mathbf{Z}_1(\mathbf{k}) &= (z_{s_{x^2+y^2}}, z_{d_{x^2-y^2}}, z_{p_x}, z_{p_y}), \\
 \mathbf{Z}_2(\mathbf{k}) &= (z_{s_{x^2y^2}}, z_{d_{xy}}, z_{p_x+p_y}, z_{p_x-p_y}), \\
 \mathbf{Z}_3(\mathbf{k}) &= \mathbf{Z}_1(2k_x, 2k_y), \quad \mathbf{Z}_6(\mathbf{k}) = \mathbf{Z}_2(2k_x, 2k_y), \\
 \mathbf{Z}_4(\mathbf{k}) &= \mathbf{Z}_2(2k_x, k_y), \quad \mathbf{Z}_5(\mathbf{k}) = \mathbf{Z}_2(k_x, 2k_y),
 \end{aligned} \tag{33}$$

and so on. The basis functions are given in Table 1 and derived in Appendix B.<sup>5</sup> Since different irreps do not mix, we can write the BdG equation Eq. (22) in the irreps basis of  $\mathbf{z}_\nu$  as

$$H = \int_{\mathbf{k}} \sum_{\nu} H_{\nu, \mathbf{z}_\nu(\mathbf{k})} |\nu, \mathbf{k}\rangle \langle \nu, \mathbf{k}|, \tag{34}$$

where the chemical potential term is included for  $\nu = 0$ .  $H_\nu$  is a  $2 \times 2$  matrix in the particle-hole basis given by

$$H_\nu = \begin{pmatrix} t_\nu & \Delta_\nu \\ \Delta_\nu^* & -t_\nu \end{pmatrix}. \tag{35}$$

( $t_\nu$  and  $\Delta_\nu$  are obtained from  $t_{\mathbf{R}}$  and  $\Delta_{\mathbf{R}}$  with the same basis transformation map employed on  $\mathbf{Z}_{d_i} = U_i \mathbf{Z}_\nu$ , as given in Table 1.)  $t_\nu$  ( $\Delta_\nu$ ) corresponds to the hopping (pairing) between a Wannier state at  $\mathbf{R}_1 = \mathbf{0}$  and the  $\nu^{\text{th}}$ -compact orbital. The non-interacting energy dispersion is  $\xi(\mathbf{k}) = \sum_{\nu} \xi_{\nu}(\mathbf{k}) = \sum_{\nu} t_{\nu, \mathbf{z}_\nu(\mathbf{k})}$ , and the gap function is  $\Delta(\mathbf{k}) = \sum_{\nu} \Delta_{\nu, \mathbf{z}_\nu(\mathbf{k})}$ . The Bogoliubov

<sup>5</sup>Note that the Wannier states in the  $\mathbf{z}_\nu$  basis can be a realization of the compact Wannier orbital [66]  $w_\nu(\mathbf{r}) = \int_{\mathbf{k}} z_\nu(\mathbf{k}) u(\mathbf{k}, \mathbf{r}) e^{i\mathbf{k}\cdot\mathbf{r}}$ .

quasiparticle energy is  $E(\mathbf{k}) = \sum_{\nu} E_{\nu}(\mathbf{k}) = \sum_{\nu} E_{\nu} z_{\nu}(\mathbf{k})$  where  $E_{\nu} = \sqrt{|t_{\nu}|^2 + |\Delta_{\nu}|^2}$ . In the SC ground state, only a single (or degenerate) irrep  $\bar{\nu}$  is present, say  $\Delta_{\bar{\nu}} \neq \mathbf{0}$ , while others are zero. In such a case, the BCS ground state energy with respect to the normal state is defined by

$$\Delta E_{\text{BCS}} = \int_{\mathbf{k}} z_{\bar{\nu}}(\mathbf{k}) [t_{\bar{\nu}} f(\xi_{\bar{\nu}}(\mathbf{k})) - E_{\bar{\nu}} f(E_{\bar{\nu}}(\mathbf{k}))] \sim -\frac{|\Delta_{\bar{\nu}}|^2}{2|t_{\bar{\nu}}|} n_{\bar{\nu}}, \quad (36)$$

where  $f$  stands for Fermi Dirac distribution function and  $n_{\bar{\nu}}$  is the filling fraction in this irrep. Therefore, only the  $\bar{\nu}$  irrep for both  $t_{\bar{\nu}}$  and  $\Delta_{\bar{\nu}}$  contribute to the BCS ground state energy. The other irreps  $t_{\nu \neq \bar{\nu}}$  determine  $\mathbf{k}_F$  and to the pairing interaction  $\Gamma(\mathbf{k}_{1,2})$  such that a  $\Delta_{\bar{\nu}} \neq \mathbf{0}$  solution is self-consistently obtained.

We focus on the tight-binding parameter space such that  $t_{\nu=\bar{\nu}} \neq \epsilon$  and  $t_{\nu \neq \bar{\nu}} = \mathbf{0}$ , where  $\epsilon$  is small compared to the interaction.  $\epsilon$  is kept small to mimic a nearly flat band. This aids an analytical solution to the SC gap equation in Eq. (32), which takes a simpler form in the irreps space as:

$$\int_{\mathbf{k}_2} \Gamma_{\bar{\nu}}^{\bar{\nu}}(\mathbf{k}_{1,2}) z_{\bar{\nu}}(\mathbf{k}_2) = -\lambda z_{\bar{\nu}}(\mathbf{k}_1). \quad (37)$$

$\Delta_{\bar{\nu}}$  drops out from both sides. Here the RPA interaction  $\Gamma_{\bar{\nu}}^{\bar{\nu}}$  is diagonal in the  $\bar{\nu}$  irrep, but not diagonal between  $\mathbf{k}_{1,2}$ . The  $\mathbf{k}$  integration is reduced to the Fermi momenta  $\mathbf{k}_F$  only, which is determined by the contour  $|z_{\bar{\nu}}(\mathbf{k}_F)| = t_{\bar{\nu}}/\mu$  where  $\mu$  is the chemical potential.<sup>6</sup> Accordingly,  $\Gamma_{\bar{\nu}}^{\bar{\nu}}(\mathbf{k}_{1,2})$  has a strong peak due to Fermi surface nesting and/or RPA instability at some nesting vector  $\mathbf{Q} = \mathbf{k}_{2F} - \mathbf{k}_{1F}$ . Then a finite pairing strength  $\lambda > \mathbf{0}$  exists if  $z_{\nu}(\mathbf{k}_{1F})$  and  $z_{\bar{\nu}}(\mathbf{k}_{1F} + \mathbf{Q})$  changes sign across the FS nesting vector. Otherwise, a SC solution does not exist for this repulsive interaction  $\Gamma > \mathbf{0}$ .<sup>7</sup>

Here, we consider several parameter ranges such that  $t_{\nu}$  is non-zero for only one irrep and others being zero. We denote  $t_i$  and  $t'_i$  as the first and second nearest neighbor shopping, see Table 1.

(i)  $t_i = \epsilon/2$ , and  $t'_i = \mathbf{0}$ . In this case  $t_{s_{x^2+y^2}} = \epsilon$ , and the rest are zero. This makes only  $\Delta_{s_{x^2+y^2}}$  pairing possible. For the single band case with either electron or hole-like FSs, where the FS centers at  $\Gamma = (\mathbf{0}, \mathbf{0})$  or  $M = (\pi, \pi)$ , the FS does not change sign. As a result, Eq. (37) does not have any non-trivial solution except  $\lambda = \mathbf{0}$ . However, a finite  $\lambda$  solution can arise for a two-band model with both electron and hole-like pockets, as observed in Fe-pnictide superconductors. [67–70].

(ii) Next consider  $t_1 = -t_2 = t_3 = -t_4 = \epsilon/2$ , which gives the only non-zero irrep is  $t_{d_{x^2-y^2}} = 2\epsilon$ . In this case, any single band FS will have a  $\lambda > \mathbf{0}$  solution. This gives a  $\Delta_{d_{x^2-y^2}}$  spin singlet pairing.

(iii) For  $t_1 = t_2 = -t_3 = -t_4$ , we have  $t_{x/y} = \pm 2\sqrt{2}\epsilon$ , while the rest is zero. Here, a single band pairing is possible only for an electron like FS, but not for any hole-doped case. Since the pairing is odd under spatial parity, the spin sector is a triplet  $\mathbf{X}_-$  in a single band case.

Next, we consider the next nearest neighbor pairing channels, promoted by the next nearest neighbor hopping  $t'_i$ . Needless to say, its difficult to obtain  $t'_i \neq \mathbf{0}$  while  $t_i = \mathbf{0}$ , unless in the flat-band limit. Therefore, the nearest-neighbor pairing does not solely appear in a system, but rather coexists with the first nearest-neighbor pairing. Here, we can similarly discuss

<sup>6</sup>Since  $z_{\nu}$  are linearly independent Bloch states at each  $\mathbf{k}$ , a flat band solution  $\xi(\mathbf{k}) = \mathbf{0}, \forall \mathbf{k}$  demands  $t_{\nu} = \mathbf{0}, \forall \nu$ . Alternatively, if one or more  $t_{\nu}$  turns out to be degenerate, a linear superposition state  $z_{\mu}(\mathbf{k}) = \sum_{\nu} C_{\nu,\mu}(\mathbf{k}) z_{\nu}(\mathbf{k})$ , while summation runs over the degenerate states, is also valid for all values of  $\mathbf{C}(\mathbf{k})$ . If there exists a function  $\mathbf{C}(\mathbf{k})$  such that  $z_{\mu}(\mathbf{k}) = \mathbf{0}, \forall \mathbf{k}$  we have a flat band.

<sup>7</sup>Note that when other  $t_{\nu} \neq \mathbf{0}$  terms contribute, the  $\mathbf{k}_F$  topology changes and, hence, the nesting profile and the nesting strength change, while the main criterion for sign reversal in the SC irrep  $z_{\bar{\nu}}$  remains the same.



$t_{s_x 2y^2} = \epsilon$  case. This gives a  $s_x 2y^2$  pairing near the half-filling where the FS is large enough to change sign. In multiband cases with different FSs possessing different sign of  $\mathbf{z}_\nu$ , we can have this pairing. (v) For  $t'_{d_{xy}} = \epsilon$  while others are zero, we have a  $d_{xy}$  pairing near half-filling. (vi) Finally, in rare events of  $t'_{p_x \pm p_y} = \epsilon$ , we have an exotic  $p_{x \pm y}$  pairing state for small electron and hole FSs, but not near the half-filling. All the conclusions are also summarized in Table 1.

### 3.2 Bogoliubov orbitals

Finally, we evaluate the Wannier-like states of the Bogoliubov quasiparticles along the line discussed in Eq. 29. Starting from the non-local Bogoliubov transformation for a single band case,  $U_{R_1} H_{R_{1,2}} U_{R_2}^\dagger = -D_{R_{1,2}}$ , we substitute  $\mathbf{R}_1 = \mathbf{0}$  and going to the irreps space of  $\nu$ , we have  $U H_\nu U_\nu^\dagger = -D_\nu$ , where  $H_\nu$  is given in Eq. (35) and  $D_\nu$  is the diagonal matrix whose components are  $\pm E_\nu$ . The Bogoliubov transformation is defined as  $U_\nu = (I \cos \theta_\nu + \sigma_y \sin \theta_\nu)$  with  $\tan 2\theta_\nu = -\Delta_\nu / t_\nu$  [71]. Substituting  $U_\nu$  in Eq. (29), we obtain the Bogoliubov orbital as a compact orbital in the pairing irrep  $\bar{\nu}$ .

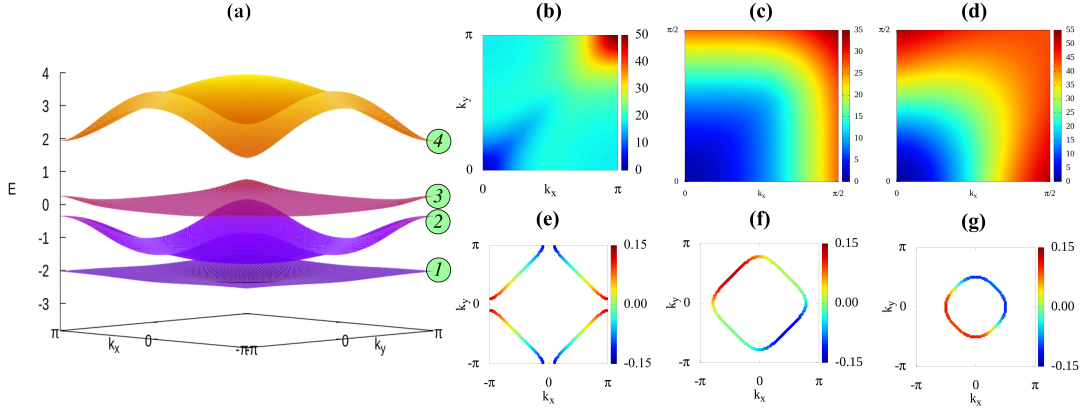


Figure 4: (a) We reproduce the band structure of the tight-binding model from Ref. [62] in 2D SO lattice. The number inside the circle enumerates the bands. We consider band-3 for further analysis of the flat band. (b-d) Static RPA susceptibility  $\text{Tr}\Pi_s(\mathbf{q})$  is plotted in the 2D BZ for three representative values of the chemical potential: (b,e)  $\mu=0.05$ , (c,f)  $\mu=0.045$  and (d,g)  $\mu=0.04$ . We plot the corresponding FS topologies for the three cases discussed in the above panels. The chemical potential is chosen to capture the metallic state on the flat band only. The gradient color gives the pairing eigenfunction  $\mathbf{z}_{\bar{\nu}}$  of Eq. (32) for the higher eigenvalue in the three cases.

### 3.3 Tight-binding model and numerical solution

To validate our analytical result, we calculate the pairing symmetry for the full four-band model [62] by tuning the chemical potential to the flat band. The reproduced band structure is shown in Fig. 4(a). We analyze three representative FS topologies: hole doping in Fig. 4(e), near half-filling in Fig. 4(f), and electron doping in Fig. 4(g). The corresponding RPA susceptibility  $\text{Tr}\Pi_s(\mathbf{q})$  in the dominant spin channel is plotted in the upper panels of Fig. 4(b-d). Pairing eigenvalues and eigenfunctions are calculated by solving the full eigenvalue equation in Eq. (32), with  $\mathbf{z}_{\bar{\nu}}$  of the highest eigenvalue is plotted as a color gradient on the FS in Fig. 4(e-g).

For large FS in the hole-doped case, the FS nesting is dominated near  $\mathbf{q}_1 = (\pi, \pi)$ , leading to a sign-reversing  $\mathbf{z}_{d_{x^2-y^2}}$  pairing symmetry, as discussed in Fig. 3(b). In the electron-doped

case, the squarish FS of the near flat bands, shifts the nesting wavevector to  $\mathbf{q}_2 = (\pi, 0)/(0, \pi)$ , as seen in Fig. 4(d). This prompts a  $\mathbf{z}_{p_{x/y}}$  pairing state, as confirmed by numerical results plotted in Fig. 4(g).

At the critical point near half-filling, where  $\mathbf{q}_1$  and  $\mathbf{q}_2$  nestings are degenerate, an intriguing question arises: do the  $\mathbf{z}_{d_{x^2-y^2}}$  and  $\mathbf{z}_{p_{x/y}}$  pairings coexist or compete? Since they belong to different irreps and different fermion parity sectors, their coexistence requires lifting spin degeneracy (by spin-orbit coupling) or lattice symmetry breaking. [54] Another possibility is a quantum liquid-like phase involving disorder mixtures of the two pairing symmetries, as proposed in ReHf<sub>2</sub> [72]. Alternatively, a first-order phase transition separates the two pairings, as seen in Sr<sub>0.1</sub>Bi<sub>2</sub>Se<sub>3</sub> [73]. However, it is worth noting that exact degeneracy between the two nestings occurs only in the ideal flat-band limit. Any small dispersion breaks this degeneracy, making one of the pairings energetically favorable.

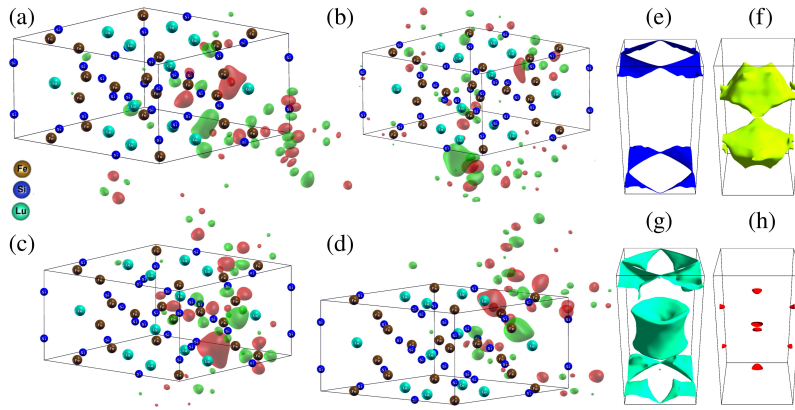


Figure 5: (a-d) Wannier functions calculated using random projections via the selected columns of the density matrix (SCDM) method [74, 75]. (e-h) show the Fermi surface reproduced from the Wannier functions.

### 3.4 First-principles calculations

Next, we extend the analysis to a multiband Wannier orbital case in the tetragonal phase of Lu<sub>2</sub>Fe<sub>3</sub>Si<sub>5</sub>. Figure 6 shows the tetragonal structure Lu<sub>2</sub>Fe<sub>3</sub>Si<sub>5</sub> with the space group  $P4/mnc$  (No. 128). The details of the crystal structure, symmetry and DFT calculations are given in Appendix C. The calculated band structure with various Fe- $\mathbf{d}$  orbital weights is shown in Fig. 7(a). Notably, the  $\mathbf{d}_{z^2}$  and  $\mathbf{d}_{xz}/\mathbf{d}_{yz}$  orbitals have larger weights near the Fermi level compared to other in-plane  $\mathbf{d}$  orbitals. This indicates the strong three-dimensional character of this material, along with pronounced FS anisotropy along the  $\mathbf{k}_z$  directions, Fig. 7(b). As analyzed in Sec. 3, especially in the Hamiltonian in Eq.(34), the larger hopping along the  $\mathbf{z}$ -direction will tend to select the pairing symmetry along the same  $\mathbf{k}_z$  direction.

We obtain the Wannier orbital for the four bands using the Wannier90 program [76]. The results are shown in Fig. 5. Expectedly, we notice that due to strong  $\mathbf{k}_z$  anisotropy and basal plane isotropy, the Wannier orbitals also have similar  $\mathbf{k}_z$  anisotropy. We find that the four Wannier orbitals have  $\mathbf{s}_{z^2}$  and  $\mathbf{d}_{z^2}$  orbital symmetries.

Due to its multiband nature, an analytical analysis of the pairing symmetry along the line presented in Sec. 3 is cumbersome. Instead, we numerically evaluate the eigenvalues of the interaction vertex  $\Gamma$  in Eq. (32). This is equivalent to calculating the expectation values of  $\Gamma$  for the symmetry-allowed pairing symmetries  $\mathbf{z}_\nu$  of a given lattice. We consider onsite and first nearest-neighbor pairing irreps of the  $D_{4h}$  group of Lu<sub>2</sub>Fe<sub>3</sub>Si<sub>5</sub>, which turn out to be  $s$  (onsite),  $\mathbf{s}_{x^2+y^2}$ ,  $\mathbf{d}_{x^2-y^2}$ ,  $\mathbf{s}_{z^2}$ ,  $\mathbf{p}_{x/y/z}$  (see Appendix B). Our results reveal two degenerate eigenvalues  $\lambda_s$

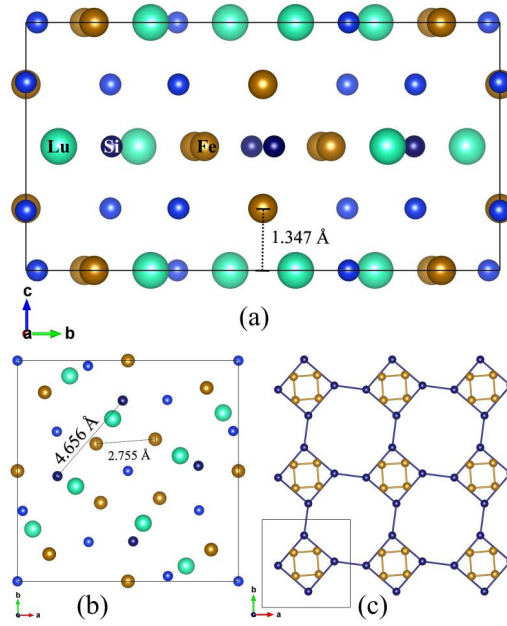


Figure 6: (a,b) Side (top) view of the  $\text{Lu}_2\text{Fe}_3\text{Si}_5$  unit-cell. The Si atoms that form the square-octagon (SO) lattice are highlighted by dark blue color. The two Si atoms of the square-octagon lattice are separated by  $4.656 \text{ \AA}$ . (c) A 2D view of the SO lattice formed by Si atoms is shown here. Each square of Si holds a square of Fe atoms. The distance between these Fe atoms is  $2.755 \text{ \AA}$ .

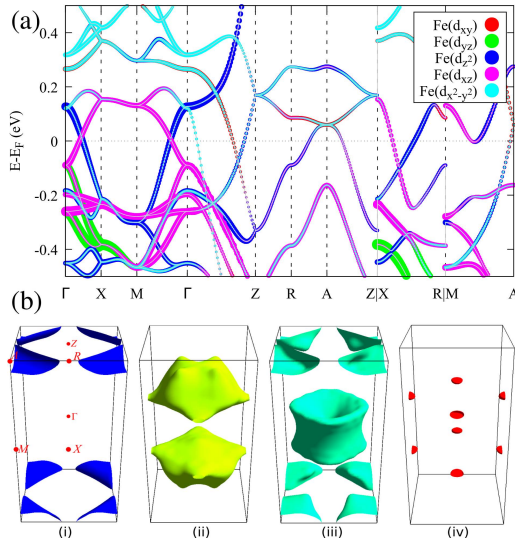


Figure 7: (a) Calculated band structure and projected orbitals weight of Fe- $d$  orbitals are shown here. The contribution from other orbitals of Fe and other atoms is negligibly small near the Fermi level. (b) The Fermi surfaces of the  $\text{Lu}_2\text{Fe}_3\text{Si}_5$  is composed of four bands, which we label as band 1,2,3 and 4. Band 1 has a negligibly small FS. Here the colors have no meaning except to distinguish different bands.

between bands 1 and 3, and  $\lambda_{s_{z^2}}$  for band 2 (see Fig. 8).

The  $s$  pairing is isotropic within each band but it changes sign between band-1 and 3, satisfying the sign-reversal requirement for a non-trivial solution of Eq. (32). Such a pairing is called  $s^\pm$  pairing, as in the iron-pnictide superconductors [67–70]. The  $s_{z^2}$  pairing in band-2

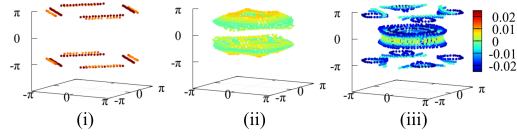


Figure 8: Pairing eigenfunctions for the higher eigenvalues for the solution of Eq. (32) are shown on the three FS. From the gradient color maps, it is evident that the gap function changes sign between bands 1 and 3 with very weak momentum anisotropy, which we attribute to  $s^\pm$  pairing symmetry. The colormap for band 2 suggests that it's a  $s_{z^2}$  pairing symmetry.

originates from its intraband FS nesting along the  $k_z$ -direction, leading to SC gap nodes on the  $k_z = \pm\pi/2$  planes. This axial pairing symmetry, driven by the same-symmetric Wannier orbital ( $s_{z^2}$ ) was also predicted and subsequently confirmed in infinite-layer nickelate superconductors. [77]. Our finding of band resolved two  $s$ -wave pairings is consistent with the penetration depth data fitted with  $s + s$  pairing symmetry in  $\text{Lu}_2\text{Fe}_3\text{Si}_5$  compounds. [29] The coexistence of two sign-reversal pairing gaps leads to multiple magnetic resonance peaks arising from magnetic fluctuations of distinct Cooper pairs [78] and can be detected by inelastic neutron scattering measurements.

## 4 Conclusions

We dedicated most of this paper in developing a formalism for constructing lattice model which can be applied to non-interacting band structure, many-body ground states, and systems coupled to a bath. Instead of relying on localized real-space orbitals corresponding to Bloch states, our approach begins with describing states, operators, and fields in phase space, and the final results are then projected onto the desired real or momentum space. Notably, we do not treat the full real and momentum spaces as a single phase-space manifold. Instead, we work within the momentum space, embedding the real-space within the Bloch vector space at each momentum point. Orbital and spin states are included by forming trivial product state with the Bloch vector, while the quantum statistics, topology, and entanglements are derived from the Hamiltonian. This approach offers several advantages: (i) The localization and uncertainty of states in real and momentum space are inherently fixed. (ii) The method bypasses any obstruction between the global and local properties defined in the momentum and real space, as they are included via unitary rotation and projection operators on the phase space.

For demonstrations and applications of the framework, we focussed on the superconductivity in SO materials. We first analyzed a single flat-band case, showcasing the framework's effectiveness in analytically solving unconventional pairing symmetries within a spin-fluctuation mechanism. A key finding is that while the superconducting ground state exhibits global coherence across all bands in momentum space, the pairing symmetry is dictated by compact orbitals aligned with the irreps of the underlying lattice symmetry.

Next we applied the method on the SO material  $\text{Lu}_2\text{Fe}_3\text{Si}_5$  with the DFT band structure and Wannier orbitals. We found that the interplay between the multibands and three-dimensionality produces Wannier orbitals of corresponding symmetries. We observed the coexistence of uniform  $s^\pm$  pairing across two bands and a nodal  $s_{z^2}$  symmetry for a third band.

While our application focussed on studying unconventional pairings, the presentation of the method was kept general for future studies into other exotic many-body states. The method can be viewed as a variational approach with variational parameters include single quasiparticles excitations for a Fermi liquid state, density wave orders for symmetry-breaking phases, or

even exotic Bell pairs or Cooper pairs or entangled pairs for spin liquid or fractional quantum Hall states. This flexibility opens new possibilities, such as: (i) Assigning quantum statistics and braiding phases to orbitals and Bloch vectors, respectively, as variational parameters. (ii) Modeling fractional quantum Hall or fractional Chern states by attaching vortices in Bloch vector space to orbital states. (iii) Stabilizing liquid states of compact orbitals in flat-band degenerate manifolds or spin-singlet liquids in quantum spin-liquid metals. These and other possibilities remain open for future exploration.

## Acknowledgements

R.S. acknowledges the Science and Engineering Research Board (SERB), Government of India, for providing the NPDF fellowship with grant number PDF/2021/000546. T.D. acknowledges funding from Core Research Grant (CRG) of S.E.R.B. (CRG/2022/003412), under I.R.H.EA Grant (IPA/2020/000034) and benefited from the computational resources (SERC) from the Indian Institute of Science.

## A Density-Density interaction and Random Phase Approximation (RPA)

The explicit expression for the onsite interactions, given in Eq. (14), can be written from Eq. (12) in terms of the density fields defined in Eqs. (7) and (5) as

$$\begin{aligned}
U_n &= V_{nn}^{nn} V_{ss}^{\bar{s}\bar{s}} = \int_{\mathbf{r}_{1,2}} V_{00,nn,ss}^{00,nn,\bar{s}\bar{s}}(\mathbf{r}_{1,2}) \mathcal{W}_{nn}(\mathbf{r}_1) \mathcal{W}_{nn}(\mathbf{r}_2) \mathcal{X}_{ss} \mathcal{X}_{\bar{s}\bar{s}}, \\
U'_{mn} &= V_{nn}^{mm} V_{ss}^{tt} = \int_{\mathbf{r}_{1,2}} V_{00,nn,ss}^{00,mm,tt}(\mathbf{r}_{1,2}) \mathcal{W}_{nn}(\mathbf{r}_1) \mathcal{W}_{mm}(\mathbf{r}_2) \mathcal{X}_{ss} \mathcal{X}_{tt}, \\
J_{mn} &= V_{nn}^{mm} V_{st}^{st} = \int_{\mathbf{r}_{1,2}} V_{00,nn,st}^{00,mm,st}(\mathbf{r}_{1,2}) \mathcal{W}_{mm}(\mathbf{r}_1) \mathcal{W}_{nn}(\mathbf{r}_2) \mathcal{X}_{st} \mathcal{X}_{st}, \\
J'_{mn} &= V_{nm}^{nm} V_{ss}^{\bar{s}\bar{s}} = \int_{\mathbf{r}_{1,2}} V_{00,nm,ss}^{00,nm,\bar{s}\bar{s}}(\mathbf{r}_{1,2}) \mathcal{W}_{nn}^*(\mathbf{r}_1) \mathcal{W}_{mm}(\mathbf{r}_2) \mathcal{X}_{\bar{s}\bar{s}}^* \mathcal{X}_{\bar{s}\bar{s}} \quad (38)
\end{aligned}$$

It is convenient to express the abstract states and the matrix elements of the operators in the second quantized form. Introducing the creation operator in the Wannier basis as  $|\mathbf{R}n s\rangle = \mathbf{c}_{\mathbf{R}n s}^\dagger |\mathbf{G}\rangle$ , where  $|\mathbf{G}\rangle$  is the many-body ground state serving as a vacuum to the low-energy excitations. Note that here, the orbital's Wyckoff position  $\mathbf{r}$  does not enter into the abstract states as they are included in the wavefunctions  $w_n(\mathbf{r})$ . The corresponding field operator is defined as  $\psi_{ns}^\dagger(\mathbf{r}) = \sum_{\mathbf{R}} w_n(\mathbf{r}) \mathbf{c}_{\mathbf{R}n s}^\dagger$ . The local densities are defined as  $n_{\mathbf{R}n s} = \mathbf{c}_{\mathbf{R}n s}^\dagger \mathbf{c}_{\mathbf{R}n s}$ , we obtain the charge density as  $n_{\mathbf{R}n} = \frac{1}{2} \sum_s n_{\mathbf{R}n s}$ , spin operator  $\mathbf{S}_{\mathbf{R}n} = \frac{1}{2} \sum_{st} \mathbf{c}_{\mathbf{R}n s}^\dagger \boldsymbol{\sigma}_{st} \mathbf{c}_{\mathbf{R}n t}$ , and pair operator  $\zeta_{\mathbf{R}n} = P_\theta \sum_s \mathbf{c}_{\mathbf{R}n s} \mathbf{c}_{\mathbf{R}n \bar{s}}$ . We write Eq. (11) by substituting Eqs. (39) as

$$H_V = \sum_{\mathbf{R}n s} U_n n_{\mathbf{R}n s} n_{\mathbf{R}n \bar{s}} + \sum_{\mathbf{R}, n < m} \left[ (U' - J/2)_{mn} n_{\mathbf{R}m} n_{\mathbf{R}n} - 2J_{mn} \mathbf{S}_{\mathbf{R}m} \cdot \mathbf{S}_{\mathbf{R}n} + J'_{mn} \zeta_{\mathbf{R}m}^\dagger \zeta_{\mathbf{R}n} \right]. \quad (39)$$

This is the famous Hubbard-Kanamori interaction Hamiltonian in a multiband system [41]. To derive the RPA interaction as many-body renormalized interaction due to density-density fluctuations, we express Eq. (39) in terms of generalized density-matrix and non-local interaction

form:

$$H_V(F(t)) = \sum_{\kappa_{1-4}} V_{n_{1,3}}^{n_{2,4}} \rho_{\kappa_{1,2}}^\dagger \rho_{\kappa_{3,4}} + \sum_{\kappa_{1,2}} (F_{\kappa_{1,2}}(t) \rho_{\kappa_{1,2}}(t) + \text{h.c.}), \quad (40)$$

Here we introduce a compact index  $\kappa_i \equiv (\mathbf{R}_i, \mathbf{n}_i) \equiv (\mathbf{R}_i, \mathbf{n}_i, \mathbf{s}_i)$ . (For local interaction  $\mathbf{R}_{1,4} = \mathbf{0}$ ,  $\mathbf{V}$  is identified with  $\mathbf{U}, \mathbf{U}', \mathbf{J}, \mathbf{J}'$  defined in Eq. (38). The diagonal elements in the orbital indices of the density matrix  $\rho_{\kappa_{1,2}} \delta_{\kappa_{1,2}}$  correspond to the densities ( $n_{\kappa_1}, \mathbf{S}_{\kappa_1}^{xyz}$ , and  $\zeta_{\kappa_1}$ ) in Eq. (39). We include  $F_{\kappa_{1,2}}(t)$  as an external source term that causes a (local) fluctuation to the corresponding density matrix  $\rho_{\kappa_{1,2}}$ , and it then spreads over the entire lattice due to the interaction term  $\Gamma$  and the one-body hopping term ( $H_T$ ). The  $F_{\kappa_{1,2}}(t)$  term drops out from the final result within the linear response theory.

The induced local density to the perturbation  $F_{\kappa_{1,2}}(t)$  is  $\rho_{\kappa_{1,2}}^{(\text{ind})}(t) = \rho_{\kappa_{1,2}}(F(t)) - \rho_{\kappa_{1,2}}(F=0)$ . Within RPA,  $\rho_{\kappa_{1,2}}^{(\text{ind})}(t)$  takes a *mean* value, i.e., it is a *c*-number. Substituting this in the interaction term, we obtain a non-interacting term  $\rho_{\kappa_{1,2}}^\dagger \rho_{\kappa_{3,4}} \rightarrow -(\rho_{\kappa_{1,2}}^\dagger \rho_{\kappa_{3,4}}^{(\text{ind})} + \text{h.c.}) + |\rho^{(\text{ind})}|^2 + \mathcal{O}(\rho^2)$ , where  $|\rho^{(\text{ind})}|^2$  is a number that shifts the energy, and we neglect the quadratic term in the density with respect to the mean value. Substituting this mean-field expansion in Eq. (40), we define an effective force experienced by the density as  $F_{\kappa_{1,2}}^{(\text{tot})}(t) = F_{\kappa_{1,2}}(t) + \sum_{\kappa_{3,4}} V_{n_{1,3}}^{n_{2,4}} \rho_{\kappa_{3,4}}^{(\text{ind})}(t)$ . Then, using linear response theory, we define as

$$\begin{aligned} \rho_{\kappa_{1,2}}^{(\text{ind})}(t) &= -i \int_{t'} \sum_{\kappa_{3,4}} \Pi_{\kappa_{1,3}}^{(0)\kappa_{2,4}}(t-t') F_{\kappa_{3,4}}(t'), \\ &= -i \int_{t'} \sum_{\kappa_{3,4}} \Pi_{\kappa_{2,4}}^{\kappa_{1,3}}(t-t') F_{\kappa_{3,4}}^{(\text{tot})}(t'). \end{aligned} \quad (41)$$

$\Pi, \Pi^{(0)}$  are the RPA and non-interacting density-density correlation functions, which can now be related to each other as  $\Pi_{s/c} = \Pi^{(0)} [\mathbf{I} \mp \mathbf{V} \Pi^{(0)}]^{-1}$ , where  $\Pi, \mathbf{V}$  denote square matrices defined by the (2,2)- tensor. Subscript 's' corresponds to the spin fluctuation  $\rho \equiv \mathbf{S}^\pm = \mathbf{S}_x \pm i\mathbf{S}_y$  term, and 'c' corresponds to  $\rho \equiv n, \mathbf{S}_z, \zeta$  density matrices. The bare density-density correlator is defined in the Wannier basis as  $(\Pi^{(0)})_{\kappa_{1,3}}^{\kappa_{2,4}}(t-t) = -i\theta(t-t') \langle [\rho_{\kappa_{1,3}}(t), \rho_{\kappa_{2,4}}(t')] \rangle_0$ , where  $\theta$  is the step function for retarded response,  $[\cdot, \cdot]$  corresponds to a commutator, and  $\langle \dots \rangle_0$  gives the expectation value in the ground state of the non-interacting Hamiltonian. The Fourier transformation of the susceptibility to the momentum space is given by  $[\Pi^{(0)}(\mathbf{q}, \omega)]_{n_{1,3}}^{n_{2,4}} = \sum_{\mathbf{R}_{1,2}} \int_t e^{i\omega t} (\Pi^{(0)})_{\kappa_{1,3}}^{\kappa_{2,4}}(t-t) \mathbf{z}_{\mathbf{R}_1 - \mathbf{R}_2}(\mathbf{q})$ . In the absence of SOC or superconductivity or magnetism in the non-interacting Hamiltonian, the only term in the bare susceptibility that contributes is the particle-hole susceptibility, i.e. the so-called Lindhard functions defined for the multiband case as

$$\begin{aligned} [\Pi^{(0)}(\mathbf{q}, \omega)]_{n_{13}}^{n_{24}} &= - \sum_{\mathbf{k}, \alpha_{12}} \frac{f(\xi_{\alpha_1}(\mathbf{k} + \mathbf{q})) - f(\xi_{\alpha_2}(\mathbf{k}))}{\omega + \xi_{\alpha_1}(\mathbf{k} + \mathbf{q}) - \xi_{\alpha_2}(\mathbf{k}) + i\epsilon} \\ &\quad \times S_{n_1, \alpha_1}^\dagger(\mathbf{k} + \mathbf{q}) S_{n_2, \alpha_2}^\dagger(\mathbf{k}) S_{n_3, \alpha_1}(\mathbf{k} + \mathbf{q}) S_{n_4, \alpha_2}(\mathbf{k}). \end{aligned} \quad (42)$$

We denote  $\xi_{\alpha_i}(\mathbf{k})$  as the  $\alpha_i$ -th-eigenvalue of  $H_T(\mathbf{k})$ , and  $S(\mathbf{k})$  as the unitary matrix consisting of the corresponding eigenvectors defined in Eq. (25). Finally, we obtain the effective (many-body) interaction term within the RPA, which is obtained by summing over the bubble (for density fluctuations) and ladder (for pair density fluctuations) diagrams as

$$\begin{aligned} \Gamma_{\mathbf{R}_{13}, n_{13}}^{\mathbf{R}_{24}, n_{24}} &= V_{n_{13}}^{n_{24}} - \frac{1}{2} \sum_{n_{5-8}} \text{sgn}[s_5 s_6] \mathcal{D}_{s_5} \delta_{s_5, \bar{s}_7} \delta_{s_6, \bar{s}_8} V_{n_{15}}^{n_{26}} (\Pi_s)_{\mathbf{R}_{13}, n_{57}}^{\mathbf{R}_{24}, n_{68}} V_{n_{73}}^{n_{84}} \\ &\quad - \frac{1}{2} \sum_{n_{5-8}} \delta_{s_5, s_7} \delta_{s_6, s_8} V_{n_{15}}^{n_{26}} (\Pi_c)_{\mathbf{R}_{13}, n_{57}}^{\mathbf{R}_{24}, n_{68}} V_{n_{73}}^{\alpha_{84}}. \end{aligned} \quad (43)$$

where  $\mathcal{D}_s = 2s(s+1)$  is the spin degeneracy factor.  $\text{sgn}[s_5 s_6]$  arise from the Fermion parity.

## B Example for Implementation of Fermion Parity

We demonstrate the above construction for two orbitals with spin-1/2 case on a tetragonal lattice ( $D_4$  group). For spins, the even and odd states are simply the triplets and singlet, respectively. This transformation is simply done with a basis (unnormalized) transformation on  $\mathbb{X}$  as

$$\begin{pmatrix} \uparrow\uparrow \\ \downarrow\downarrow \\ \uparrow\downarrow \\ \downarrow\uparrow \end{pmatrix} = \frac{1}{2} \begin{pmatrix} 2 & 0 & 0 & 0 \\ 0 & 2 & 0 & 0 \\ 0 & 0 & 1 & 1 \\ 0 & 0 & 1 & -1 \end{pmatrix} \begin{pmatrix} \uparrow\uparrow \\ \downarrow\downarrow \\ \uparrow\downarrow + \downarrow\uparrow \\ \uparrow\downarrow - \downarrow\uparrow \end{pmatrix}, \quad (44)$$

which gives the corresponding unitary transformation  $U_{\theta(X)}$  in Eq. (20).

For two orbitals, we similarly define interorbital terms into even and odd parity states  $\mathbb{W}_{\pm} = 1/\sqrt{2}(w_1 w_2 \pm w_1 w_2)$ , and intraorbital states  $w_1 w_1 w_2 w_2$  are even parity. This transformation is done with a similar unitary transformation  $U_{\theta(W)}$ . These four states are also the irreps of the  $D_4$  symmetry.

For the Bloch basis  $\mathbb{Z}$ , the fermion parity becomes the same as the spatial inversion for zero-momentum Cooper pairs. We can write  $\mathbb{Z}$  as a polynomial of either (even)  $\cos(\mathbf{k} \cdot \boldsymbol{\delta})$  or (odd)  $\sin(\mathbf{k} \cdot \boldsymbol{\delta})$ , where  $\boldsymbol{\delta} = \mathbf{R}_1 - \mathbf{R}_2$ . This is easier to demonstrate with an example. Consider a  $D = 3$  - dimensional simple tetragonal lattice. The onsite pairing at  $\boldsymbol{\delta}_0 = (0, 0, 0)$  gives a trivial  $s$ -wave superconductivity. For the nearest neighbor term, we have  $d = 6$  with their distances being  $\boldsymbol{\delta}_{1,2} = (\pm 1, 0, 0)$ ,  $\boldsymbol{\delta}_{3,4} = (0, \pm 1, 0)$ ,  $\boldsymbol{\delta}_{5,6} = (0, 0, \pm 1)$ , for the lattice constants  $a = b = c = 1$ . So we have a six-dimensional Bloch spinor  $\mathbb{Z}_6(\mathbf{k}) = (e^{ik_x} e^{-ik_x} e^{ik_y} e^{-ik_y} e^{ik_z} e^{-ik_z})^T$ . Setting one electron at the origin, i.e.,  $\mathbf{R}_1 = \mathbf{0}$ , we express the two-particle Bloch spinor in terms of single particle Bloch spinor as  $\mathbb{Z}(\mathbf{k}) = z_0 \mathbb{Z}_6(\mathbf{k})$ , where  $z_0 = 1$ . More generally we can move to the irreps of the point group symmetry for  $\mathbb{Z}_6$ , which for the  $D_4$  group are trivial to find. We choose (unnormalized) bases as

$$\begin{aligned} |s_{x^2+y^2}\rangle &= (1 \ 1 \ 1 \ 1 \ 0 \ 0)^T, \\ |s_{z^2}\rangle &= (0 \ 0 \ 0 \ 0 \ 1 \ 1)^T, \\ |p_x\rangle &= (1 \ -1 \ 0 \ 0 \ 0 \ 0)^T, \\ |p_y\rangle &= (0 \ 0 \ 1 \ -1 \ 0 \ 0)^T, \\ |p_z\rangle &= (0 \ 0 \ 0 \ 0 \ 1 \ -1)^T, \\ |d_{x^2-y^2}\rangle &= (1 \ 1 \ -1 \ -1 \ 0 \ 0)^T. \end{aligned} \quad (45)$$

These bases constitute the unitary transformation  $U_{\theta(Z)}$  in Eq. (20). We make two observations here. The basis states are not unique, and one needs to pay attention to the symmetry of the lattice. Secondly, the  $t_{2g}$  irrep states are not included as they arise from the second nearest neighbor pairings (as shown for square lattice in Eq. (33)). We write the corresponding Bloch wavefunctions as (up to a normalization)

$$\begin{aligned} z_{s_{x^2+y^2}}(\mathbf{k}) &= \langle s_{x^2+y^2} | \mathbb{Z}(\mathbf{k}) \rangle = \cos k_x + \cos k_y, \\ z_{s_{z^2}}(\mathbf{k}) &= \langle s_{z^2} | \mathbb{Z}(\mathbf{k}) \rangle = \cos k_z, \\ z_{p_{x/y/z}}(\mathbf{k}) &= \langle p_{x/y/z} | \mathbb{Z}(\mathbf{k}) \rangle = i \sin k_{x/y/z}, \\ z_{d_{x^2-y^2}}(\mathbf{k}) &= \langle d_{x^2-y^2} | \mathbb{Z}(\mathbf{k}) \rangle = \cos k_x - \cos k_y. \end{aligned} \quad (46)$$

Note that these functions are the eigenstates of the fermion parity  $P_{\theta(z)}$  being  $+1$  for  $s$ - and  $d$ - waves and  $-1$  for  $p$ -wave states.

## C First-principles electronic structure calculations

We used first-principles electronic structure calculations to examine the band structure and the Fermi surface of the system to understand the origins of multiband superconductivity in  $\text{Lu}_2\text{Fe}_3\text{Si}_5$ . We perform density functional theory (DFT) simulation using the Vienna Ab initio Simulation Package (VASP) [79, 80]. For the exchange-correlation between electrons, we employed the generalized gradient approximation (GGA), parametrized by Perdew–Burke–Ernzerhof (PBE) [81]. We employed the projector–augmented wave (PAW) approach to characterize the interaction between the core and valence electrons [82, 83]. The plane–wave energy cutoff is set at 400 eV. The Brillouin zone (BZ) is sampled using the Monkhorst–Pack technique [84] with a grid spacing of 0.01 for all calculations, which yields equivalent  $29 \times 29 \times 29$  and  $30 \times 30 \times 3$  k-point meshes for Rhombohedral and Hexagonal unitcells, respectively. The structural relaxation was carried out until the forces acting on each atoms were less than 0.0001 eV/Å. The convergence threshold for energy in the electronic self–consistent cycle was set to  $10^{-8}$  eV. The simplified method suggested by Dudarev et al. [85] was used to make the PBE+U calculations, which simply considers the difference of  $U$  and  $J$  ( $U_{\text{eff}} = U - J$ ). The value of  $U_{\text{eff}}$  for Fe  $3d$  was set at 4.0 eV [86], while it is zero for the other atoms. We also performed the spin–orbit coupling (SOC) calculations.

The lattice parameters of the relaxed structure are  $a = b = 10.2898$  Å and  $c = 5.3884$  Å. This structure consisting of two-dimensional iron squares perpendicular to the  $c$  axis as shown in the Fig. 6(a). Each iron plane is separated by a distance of 1.3471 Å and contains silicon atoms. The central silicon plane forms a square-octagon lattice, and within each silicon squares have iron square. The distance between silicon atoms in the squares is 4.656 Å and between irons are 2.755 Å as shown in the Fig. 6(b). Figure 6 shows the  $3 \times 3 \times 1$  sheet containing Si and Fe atoms from the central layer. Si atoms forms the square-octagon lattice. All the crystal structures shown in here were created using VESTA software [87].

The band structure of  $\text{Lu}_2\text{Fe}_3\text{Si}_5$  is dominated by Fe  $3d$  electrons and exhibits a 3D configuration with electron-like and hole-like sheets. Figure 7(a) shows the band diagram of  $\text{Lu}_2\text{Fe}_3\text{Si}_5$  with the weights of the various Fe  $3d$  orbitals. We also calculated the spin-polarized band structure, which was found to be spin-degenerate, suggesting the non-magnetic nature of Fe atoms in this system. Therefore, we did not apply spin-orbit coupling. We found that four bands (122, 123, 124, and 125) cross the Fermi level, among which bands 122 and 123 are electron-like, and the remaining ones are hole-like. Both hole-like bands are degenerate at the high-symmetry point  $A$  of the BZ, where they form a dome. This portion of the band diagram is dominated by the Fe  $3d_{z^2}$  orbital with some contributions from the  $d_{xz}$  and  $d_{x^2-y^2}$  orbitals near the Fermi surface. Both electron-like bands cross the Fermi surface along  $\Gamma - Z$  and  $X - R$ , with contributions from the Fe  $3d_{x^2-y^2}$ ,  $d_{xy}$ ,  $d_{z^2}$ , and  $d_{xz}$  orbitals. The interactions between different orbitals and their contributions to the electronic structure can result in the emergence of multiple Fermi surface sheets and potentially lead to complex multiband superconductivity.

The Fermi surface of  $\text{Lu}_2\text{Fe}_3\text{Si}_5$  is composed of several bands originating from mainly three distinct branches labeled as i-iii in Figure 7(b). Each of these bands possesses specific features that play a crucial role in the superconducting state of the compound. This Fermi surface exhibits both hole-like and electron-like characteristics within its topology. Notably, FS pockets i and iii exhibit a hole-like nature, while FS sheet ii is electron-like. In FS pockets i and iii, there are pockets centered at the corner ( $A$ ) of the Brillouin Zone (BZ) with a quasi-2D structure.



Conversely, the electron-like Fermi surface sheet ii takes on a three-dimensional form, resembling a roughly spherical shape positioned along the  $\Gamma - Z$  path. Moreover, FS sheet iii also displays the 3D pocket that takes on a cylindrical form centered around the  $\Gamma$  point. These Fermi surface sheets confirm the fulfillment of conditions for multi-band superconductivity in  $\text{Lu}_2\text{Fe}_3\text{Si}_5$ . This finding is in good agreement with previous works [27, 88, 89].

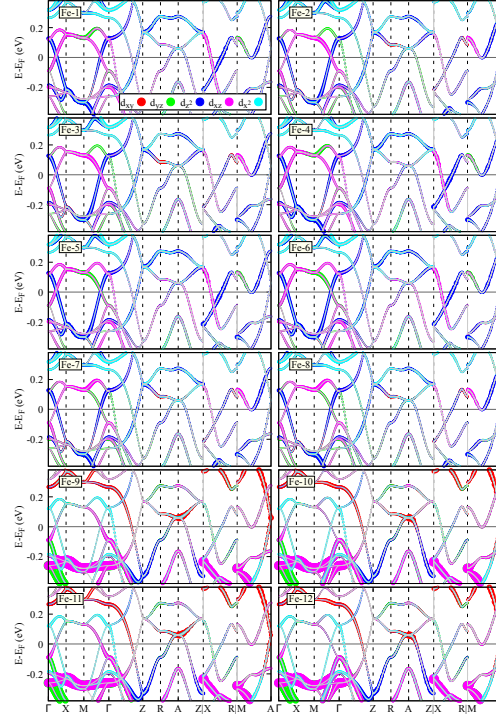


Figure 9: Projected bands of all Fe atoms are depicted, with the weight of  $d$  orbitals varying according to the symbol size. The colors represent different  $d$  orbitals. The vertical dashed lines indicate the high-symmetry points of the BZ, and the gray horizontal line represents the offset of the Fermi energy to zero. The legend is displayed in the top-left sub-figure. Fe-i represents the label of Fe atoms.

In Figure 9, we present the projected band structure of all Fe atoms in the unit cell, highlighting the weight of Fe  $3d$  orbitals using symbol size. Upon inspecting Fig. 9, we observe that for Fe-1 and Fe-4, the  $d_{xz}$  and  $d_{z^2}$  orbitals contribute predominantly near the Fermi level. For Fe-2 and Fe-3, the  $d_{xz}$ ,  $d_{z^2}$ , and  $d_{yz}$  orbitals exhibit significant contributions. Similarly, for Fe-5 to Fe-8, the  $d_{xz}$ ,  $d_{z^2}$ , and  $d_{yz}$  orbitals play a major role, with a larger weight of  $d_{yz}$  observed for Fe-7 and Fe-8. In the case of Fe-9 to Fe-10, the  $d_{xz}$ ,  $d_{x^2}$ ,  $d_{xy}$ , and  $d_{yz}$  orbitals predominantly contribute, while Fe-10 and Fe-12 exhibit a higher weight of  $d_{xz}$  compared to others. Recall the positions of Fe atoms in the unit-cell, Fe-5 to Fe-8 form the central layer along the  $c$  axis, while Fe-1 to Fe-4 constitute the outer layers. Fe-9 to Fe-12 are sandwiched between the outer and central layers of Fe. The central layer of Fe, which forms a square, has a contribution from the  $d_{z^2}$  orbital, whereas the sandwiched layer, which does not form a square, has no contribution from the  $d_{z^2}$  orbital but exhibits the  $d_{x^2}$  orbital.

## References

- [1] N. Marzari, A. A. Mostofi, J. R. Yates, I. Souza and D. Vanderbilt, *Maximally localized wannier functions: Theory and applications*, Reviews of Modern Physics **84**, 1419 (2012),

- doi:[10.1103/RevModPhys.84.1419](https://doi.org/10.1103/RevModPhys.84.1419).
- [2] N. Marzari and D. Vanderbilt, *Maximally localized generalized wannier functions for composite energy bands*, Physical Review B **56**, 12847 (1997), doi:[10.1103/PhysRevB.56.12847](https://doi.org/10.1103/PhysRevB.56.12847).
  - [3] I. Souza, N. Marzari and D. Vanderbilt, *Maximally localized wannier functions for entangled energy bands*, Physical Review B **65**, 035109 (2001), doi:[10.1103/PhysRevB.65.035109](https://doi.org/10.1103/PhysRevB.65.035109).
  - [4] A. A. Soluyanov and D. Vanderbilt, *Wannier representation of  $z_2$  topological insulators*, Physical Review B **83**, 035108 (2011), doi:[10.1103/PhysRevB.83.035108](https://doi.org/10.1103/PhysRevB.83.035108).
  - [5] Y.-L. Wu, N. Regnault and B. A. Bernevig, *Gauge-fixed wannier wave functions for fractional topological insulators*, Physical Review B **86**, 085129 (2012), doi:[10.1103/PhysRevB.86.085129](https://doi.org/10.1103/PhysRevB.86.085129).
  - [6] G. W. Winkler, A. A. Soluyanov and M. Troyer, *Smooth gauge and wannier functions for topological band structures in arbitrary dimensions*, Physical Review B **93**, 035453 (2016), doi:[10.1103/PhysRevB.93.035453](https://doi.org/10.1103/PhysRevB.93.035453).
  - [7] D. Gresch, G. Autès, O. V. Yazyev, M. Troyer, D. Vanderbilt, B. A. Bernevig and A. A. Soluyanov, *Z2pack: Numerical implementation of hybrid wannier centers for identifying topological materials*, Physical Review B **95**, 075146 (2017), doi:[10.1103/PhysRevB.95.075146](https://doi.org/10.1103/PhysRevB.95.075146).
  - [8] H. D. Cornean and D. Monaco, *On the construction of wannier functions in topological insulators: the 3d case*, Annales Henri Poincaré **18**, 3863 (2017), doi:[10.1007/s00023-017-0621-y](https://doi.org/10.1007/s00023-017-0621-y).
  - [9] H. C. Po, H. Watanabe and A. Vishwanath, *Fragile topology and wannier obstructions*, Physical Review Letters **121**, 126402 (2018), doi:[10.1103/PhysRevLett.121.126402](https://doi.org/10.1103/PhysRevLett.121.126402).
  - [10] V. I. Anisimov, D. E. Kondakov, A. V. Kozhevnikov, I. A. Nekrasov, Z. V. Pchelkina, J. W. Allen, S.-K. Mo, H.-D. Kim, P. Metcalf, S. Suga, A. Sekiyama, G. Keller *et al.*, *Full orbital calculation scheme for materials with strongly correlated electrons*, Physical Review B **71**, 125119 (2005), doi:[10.1103/PhysRevB.71.125119](https://doi.org/10.1103/PhysRevB.71.125119).
  - [11] F. Lechermann, A. Georges, A. Poteryaev, S. Biermann, M. Posternak, A. Yamasaki and O. K. Andersen, *Dynamical mean-field theory using wannier functions: A flexible route to electronic structure calculations of strongly correlated materials*, Physical Review B **74**, 125120 (2006), doi:[10.1103/PhysRevB.74.125120](https://doi.org/10.1103/PhysRevB.74.125120).
  - [12] T. Das, R. S. Markiewicz and A. Bansil, *Intermediate coupling model of the cuprates*, Adv. Phys. **63**(3), 151 (2014), doi:[10.1080/00018732.2014.940227](https://doi.org/10.1080/00018732.2014.940227).
  - [13] F. Freimuth, S. Blügel and Y. Mokrousov, *Construction of wannier functions from the spectral moments of correlated electron systems* (2023), [2301.04734](https://arxiv.org/abs/2301.04734).
  - [14] D. Vollhardt, *Dynamical mean-field theory of strongly correlated electron systems*, doi:[10.7566/JPSCP30.011001](https://doi.org/10.7566/JPSCP30.011001) (2020).
  - [15] R. Boyack, L. Delacrétaz, É. Dupuis and W. Witczak-Krempa, *Conformal field theories in a magnetic field*, Phys. Rev. Res. **6**(4), 043093 (2024), doi:[10.1103/PhysRevResearch.6.043093](https://doi.org/10.1103/PhysRevResearch.6.043093).

- [16] N. Read, *Compactly supported Wannier functions and algebraic K-theory*, Phys. Rev. B **95**(11), 115309 (2017), doi:[10.1103/PhysRevB.95.115309](https://doi.org/10.1103/PhysRevB.95.115309), [1608.04696](https://arxiv.org/abs/1608.04696).
- [17] F. Schindler, B. Bradlyn, M. H. Fischer and T. Neupert, *Pairing Obstructions in Topological Superconductors*, Phys. Rev. Lett. **124**(24), 247001 (2020), doi:[10.1103/PhysRevLett.124.247001](https://doi.org/10.1103/PhysRevLett.124.247001), [2001.02682](https://arxiv.org/abs/2001.02682).
- [18] T. B. Wahl, H.-H. Tu, N. Schuch and J. I. Cirac, *Projected Entangled-Pair States Can Describe Chiral Topological States*, Phys. Rev. Lett. **111**(23), 236805 (2013), doi:[10.1103/PhysRevLett.111.236805](https://doi.org/10.1103/PhysRevLett.111.236805), [1308.0316](https://arxiv.org/abs/1308.0316).
- [19] X.-L. Qi, *Generic Wave-Function Description of Fractional Quantum Anomalous Hall States and Fractional Topological Insulators*, Phys. Rev. Lett. **107**(12), 126803 (2011), doi:[10.1103/PhysRevLett.107.126803](https://doi.org/10.1103/PhysRevLett.107.126803), [1105.4298](https://arxiv.org/abs/1105.4298).
- [20] M. Nakagawa, R.-J. Slager, S. Higashikawa and T. Oka, *Wannier representation of Floquet topological states*, Phys. Rev. B **101**(7), 075108 (2020), doi:[10.1103/PhysRevB.101.075108](https://doi.org/10.1103/PhysRevB.101.075108), [1903.12197](https://arxiv.org/abs/1903.12197).
- [21] V. Gupta and B. Bradlyn, *Wannier-function methods for topological modes in one-dimensional photonic crystals*, Phys. Rev. A **105**(5), 053521 (2022), doi:[10.1103/PhysRevA.105.053521](https://doi.org/10.1103/PhysRevA.105.053521).
- [22] Q. Li, J. Dong, P. J. Ledwith and E. Khalaf, *Constraints on real space representations of chern bands* (2024), [2407.02561](https://arxiv.org/abs/2407.02561).
- [23] H. Wang, R. Shi, Z. Liu and J. Wang, *Orbital description of landau levels* (2024), [2411.13071](https://arxiv.org/abs/2411.13071).
- [24] Y. Nakajima, H. Hidaka, T. Nakagawa, T. Tamegai, T. Nishizaki, T. Sasaki and N. Kobayashi, *Two-band superconductivity featuring different anisotropies in the ternary iron silicide Lu<sub>2</sub>Fe<sub>3</sub>Si<sub>5</sub>*, Phys. Rev. B **85**(17), 174524 (2012), doi:[10.1103/PhysRevB.85.174524](https://doi.org/10.1103/PhysRevB.85.174524).
- [25] Y. Machida, S. Sakai, K. Izawa, H. Okuyama and T. Watanabe, *Enhanced Quasiparticle Heat Conduction in the Multigap Superconductor Lu<sub>2</sub>Fe<sub>3</sub>Si<sub>5</sub>*, Phys. Rev. Lett. **106**(10), 107002 (2011), doi:[10.1103/PhysRevLett.106.107002](https://doi.org/10.1103/PhysRevLett.106.107002).
- [26] T. Tamegai, Y. Nakajima, T. Nakagawa, G. J. Li and H. Harima, *Two-gap superconductivity in R<sub>2</sub>Fe<sub>3</sub>Si<sub>5</sub> (R = Lu and Sc)*, J. Phys. Conf. Ser. **150**(5), 052264 (2009), doi:[10.1088/1742-6596/150/5/052264](https://doi.org/10.1088/1742-6596/150/5/052264).
- [27] Y. Nakajima, T. Nakagawa, T. Tamegai and H. Harima, *Specific-heat evidence for two-gap superconductivity in the ternary-iron silicide Lu<sub>2</sub>Fe<sub>3</sub>Si<sub>5</sub>*, Phys. Rev. Lett. **100**(15), 157001 (2008), doi:[10.1103/PhysRevLett.100.157001](https://doi.org/10.1103/PhysRevLett.100.157001).
- [28] C. B. Vining, R. N. Shelton, H. F. Braun and M. Pelizzone, *Low-temperature heat capacity of superconducting ternary iron silicides*, Phys. Rev. B **27**(5), 2800 (1983), doi:[10.1103/PhysRevB.27.2800](https://doi.org/10.1103/PhysRevB.27.2800).
- [29] P. K. Biswas, G. Balakrishnan, D. M. Paul, M. R. Lees and A. D. Hillier, *Two-gap superconductivity in Lu<sub>2</sub>Fe<sub>3</sub>Si<sub>5</sub>: A transverse-field muon spin rotation study*, Phys. Rev. B **83**(5), 054517 (2011), doi:[10.1103/PhysRevB.83.054517](https://doi.org/10.1103/PhysRevB.83.054517).

- [30] R. T. Gordon, M. D. Vannette, C. Martin, Y. Nakajima, T. Tamegai and R. Prozorov, *Two-gap superconductivity seen in penetration-depth measurements of  $\text{Lu}_2\text{Fe}_3\text{Si}_5$  single crystals*, Phys. Rev. B **78**(2), 024514 (2008), doi:[10.1103/PhysRevB.78.024514](https://doi.org/10.1103/PhysRevB.78.024514).
- [31] H. Hidaka, Y. Nakajima and T. Tamegai, *Impurity effects in two-gap superconductor  $\text{Lu}_2\text{Fe}_3\text{Si}_5$* , Phys. C Supercond. its Appl. **470**(SUPPL.1), S619 (2010), doi:[10.1016/j.physc.2009.10.119](https://doi.org/10.1016/j.physc.2009.10.119).
- [32] T. Watanabe, H. Sasame, H. Okuyama, K. Takase and Y. Takano, *Disorder-sensitive superconductivity in the doped iron silicide superconductor  $(\text{Lu}_{1-x}\text{R}_x)_2\text{Fe}_3\text{Si}_5$  ( $\text{R}=\text{Sc}, \text{Y}, \text{and Dy}$ )*, Phys. Rev. B **80**(10), 100502 (2009), doi:[10.1103/PhysRevB.80.100502](https://doi.org/10.1103/PhysRevB.80.100502).
- [33] H. Hidaka, Y. Nakajima and T. Tamegai, *Non-magnetic impurity effect in two-gap superconductor  $\text{Lu}_2\text{Fe}_3\text{Si}_5$* , Phys. C Supercond. **469**(15-20), 999 (2009), doi:[10.1016/j.physc.2009.05.184](https://doi.org/10.1016/j.physc.2009.05.184).
- [34] H. Sasame, T. Masubuchi, K. Takase, Y. Takano and T. Watanabe, *Superconducting properties of  $\text{Lu}_2\text{Fe}_3\text{Si}_5$  with non-magnetic impurities*, J. Phys. Conf. Ser. **150**(5), 052226 (2009), doi:[10.1088/1742-6596/150/5/052226](https://doi.org/10.1088/1742-6596/150/5/052226).
- [35] A. E. Karkin, M. R. Yangirov, Y. N. Akshentsev and B. N. Goshchitskii, *Superconductivity in iron silicide  $\text{Lu}_2\text{Fe}_3\text{Si}_5$  probed by radiation-induced disordering*, Phys. Rev. B **84**(5), 054541 (2011), doi:[10.1103/PhysRevB.84.054541](https://doi.org/10.1103/PhysRevB.84.054541).
- [36] H. F. Braun, *Superconductivity of rare earth-iron silicides*, Phys. Lett. A **75**(5), 386 (1980), doi:[10.1016/0375-9601\(80\)90849-X](https://doi.org/10.1016/0375-9601(80)90849-X).
- [37] R. Sakuma, *Symmetry-adapted Wannier functions in the maximal localization procedure*, Phys. Rev. B **87**(23), 235109 (2013), doi:[10.1103/PhysRevB.87.235109](https://doi.org/10.1103/PhysRevB.87.235109), [1306.0032](https://arxiv.org/abs/1306.0032).
- [38] J. Kang and O. Vafek, *Symmetry, Maximally Localized Wannier States, and a Low-Energy Model for Twisted Bilayer Graphene Narrow Bands*, Phys. Rev. X **8**(3), 031088 (2018), doi:[10.1103/PhysRevX.8.031088](https://doi.org/10.1103/PhysRevX.8.031088), [1805.04918](https://arxiv.org/abs/1805.04918).
- [39] A. Ramires, *Nonunitary superconductivity in complex quantum materials*, J. Phys. Condens. Matter **34**(30), 304001 (2022), doi:[10.1088/1361-648X/ac6d3a](https://doi.org/10.1088/1361-648X/ac6d3a), [2202.12178](https://arxiv.org/abs/2202.12178).
- [40] K. B. Yogendra, G. Baskaran and T. Das, *Fractional Wannier Orbitals and Tight-Binding Gauge Fields for Kitaev Honeycomb Superlattices with Flat Majorana Bands* (2024), [2407.12559](https://arxiv.org/abs/2407.12559).
- [41] J. Kanamori, *Electron Correlation and Ferromagnetism of Transition Metals*, Prog. Theor. Phys. **30**(3), 275 (1963), doi:[10.1143/PTP.30.275](https://doi.org/10.1143/PTP.30.275).
- [42] A. Georges, L. de' Medici and J. Mravlje, *Strong Correlations from Hund's Coupling*, Annu. Rev. Condens. Matter Phys. **4**(1), 137 (2013), doi:[10.1146/annurev-conmatphys-020911-125045](https://doi.org/10.1146/annurev-conmatphys-020911-125045).
- [43] T. Das and K. Dolui, *Superconducting dome in  $\text{MoS}_2$  and  $\text{TiSe}_2$  generated by quasiparticle-phonon coupling*, Phys. Rev. B **91**(9), 094510 (2015), doi:[10.1103/PhysRevB.91.094510](https://doi.org/10.1103/PhysRevB.91.094510), [1411.3096](https://arxiv.org/abs/1411.3096).
- [44] D. Pines and D. Bohm, *A Collective Description of Electron Interactions: II. Collective vs Individual Particle Aspects of the Interactions*, Phys. Rev. **85**(2), 338 (1952), doi:[10.1103/PhysRev.85.338](https://doi.org/10.1103/PhysRev.85.338).

- [45] D. Bohm and D. Pines, *A collective description of electron interactions: III. Coulomb interactions in a degenerate electron gas*, Phys. Rev. **92**(3), 609 (1953), doi:[10.1103/PhysRev.92.609](https://doi.org/10.1103/PhysRev.92.609).
- [46] D. Pines, *Emergent behavior in strongly correlated electron systems*, Reports Prog. Phys. **79**(9), 092501 (2016), doi:[10.1088/0034-4885/79/9/092501](https://doi.org/10.1088/0034-4885/79/9/092501), [1601.05891](https://arxiv.org/abs/1601.05891).
- [47] M. Gell-Mann and K. A. Brueckner, *Correlation Energy of an Electron Gas at High Density*, Phys. Rev. **106**(2), 364 (1957), doi:[10.1103/PhysRev.106.364](https://doi.org/10.1103/PhysRev.106.364).
- [48] A. D. McLACHLAN and M. A. BALL, *Time-Dependent Hartree—Fock Theory for Molecules*, Rev. Mod. Phys. **36**(3), 844 (1964), doi:[10.1103/RevModPhys.36.844](https://doi.org/10.1103/RevModPhys.36.844).
- [49] J. Oddershede, *Polarization propagator calculations*, vol. 11 of *Advances in Quantum Chemistry*, pp. 275–352. Academic Press, doi:[https://doi.org/10.1016/S0065-3276\(08\)60240-3](https://doi.org/10.1016/S0065-3276(08)60240-3) (1978).
- [50] A. Szabo and N. S. Ostlund, *The correlation energy in the random phase approximation: Intermolecular forces between closed-shell systems*, J. Chem. Phys. **67**(10), 4351 (1977), doi:[10.1063/1.434580](https://doi.org/10.1063/1.434580).
- [51] Y. Zhou, W.-Q. Chen and F.-C. Zhang, *Symmetry of superconducting states with two orbitals on a tetragonal lattice: Application to LaFeAsO<sub>1-x</sub>F<sub>x</sub>*, Phys. Rev. B **78**(6), 064514 (2008), doi:[10.1103/PhysRevB.78.064514](https://doi.org/10.1103/PhysRevB.78.064514), [0806.0712](https://arxiv.org/abs/0806.0712).
- [52] J. W. Venderbos, L. Savary, J. Ruhman, P. A. Lee and L. Fu, *Pairing States of Spin- 3/2 Fermions: Symmetry-Enforced Topological Gap Functions*, Phys. Rev. X **8**(1), 011029 (2018), doi:[10.1103/PhysRevX.8.011029](https://doi.org/10.1103/PhysRevX.8.011029), [1709.04487](https://arxiv.org/abs/1709.04487).
- [53] P. M. R. Brydon, L. Wang, M. Weinert and D. F. Agterberg, *Pairing of  $j=3/2$  Fermions in Half-Heusler Superconductors*, Phys. Rev. Lett. **116**(17), 177001 (2016), doi:[10.1103/PhysRevLett.116.177001](https://doi.org/10.1103/PhysRevLett.116.177001), [1603.03376](https://arxiv.org/abs/1603.03376).
- [54] M. Sigrist and K. Ueda, *Phenomenological theory of unconventional superconductivity*, Rev. Mod. Phys. **63**(2), 239 (1991), doi:[10.1103/RevModPhys.63.239](https://doi.org/10.1103/RevModPhys.63.239).
- [55] T. Das, *Pairing symmetries of several iron-based superconductor families and some similarities with cuprates and heavy-fermions*, EPJ Web Conf. **23**, 00014 (2012), doi:[10.1051/epjconf/20122300014](https://doi.org/10.1051/epjconf/20122300014).
- [56] J. Linder and A. V. Balatsky, *Odd-frequency superconductivity*, Rev. Mod. Phys. **91**(4), 045005 (2019), doi:[10.1103/RevModPhys.91.045005](https://doi.org/10.1103/RevModPhys.91.045005), [1709.03986](https://arxiv.org/abs/1709.03986).
- [57] H. G. Suh, Y. Yu, T. Shishidou, M. Weinert, P. M. R. Brydon and D. F. Agterberg, *Superconductivity of anomalous pseudospin in nonsymmorphic materials*, Phys. Rev. Res. **5**(3), 033204 (2023), doi:[10.1103/PhysRevResearch.5.033204](https://doi.org/10.1103/PhysRevResearch.5.033204).
- [58] P. Adhikary and T. Das, *Prediction of  $f$ -wave pairing symmetry in YBa<sub>2</sub>Cu<sub>3</sub>O<sub>6+x</sub> cuprates*, Phys. Rev. B **101**(21), 214517 (2020), doi:[10.1103/PhysRevB.101.214517](https://doi.org/10.1103/PhysRevB.101.214517), [2002.07382](https://arxiv.org/abs/2002.07382).
- [59] T. Das, J.-X. Zhu and M. J. Graf, *Local suppression of the superfluid density of PuCoGa<sub>5</sub> by strong onsite disorder*, Phys. Rev. B **84**(13), 134510 (2011), doi:[10.1103/PhysRevB.84.134510](https://doi.org/10.1103/PhysRevB.84.134510).
- [60] D. Sticlet, C. Bena and P. Simon, *Spin and Majorana Polarization in Topological Superconducting Wires*, Phys. Rev. Lett. **108**(9), 096802 (2012), doi:[10.1103/PhysRevLett.108.096802](https://doi.org/10.1103/PhysRevLett.108.096802), [1109.5697](https://arxiv.org/abs/1109.5697).

- [61] S. Ray, J. Jung and T. Das, *Wannier pairs in superconducting twisted bilayer graphene and related systems*, Phys. Rev. B **99**(13), 134515 (2019), doi:[10.1103/PhysRevB.99.134515](https://doi.org/10.1103/PhysRevB.99.134515), [1804.09674](https://arxiv.org/abs/1804.09674).
- [62] B. Pal, *Nontrivial topological flat bands in a diamond-octagon lattice geometry*, Phys. Rev. B **98**(24), 245116 (2018), doi:[10.1103/PhysRevB.98.245116](https://doi.org/10.1103/PhysRevB.98.245116).
- [63] S. M. Nie, Z. Song, H. Weng and Z. Fang, *Quantum spin Hall effect in two-dimensional transition-metal dichalcogenide haeckelites*, Phys. Rev. B **91**(23), 235434 (2015), doi:[10.1103/PhysRevB.91.235434](https://doi.org/10.1103/PhysRevB.91.235434).
- [64] A. Bao, H.-S. Tao, H.-D. Liu, X. Zhang and W.-M. Liu, *Quantum magnetic phase transition in square-octagon lattice*, Sci. Rep. **4**(1), 6918 (2015), doi:[10.1038/srep06918](https://doi.org/10.1038/srep06918).
- [65] D. J. Thouless, M. Kohmoto, M. P. Nightingale and M. den Nijs, *Quantized Hall Conductance in a Two-Dimensional Periodic Potential*, Phys. Rev. Lett. **49**(6), 405 (1982), doi:[10.1103/PhysRevLett.49.405](https://doi.org/10.1103/PhysRevLett.49.405).
- [66] D. L. Bergman, C. Wu and L. Balents, *Band touching from real-space topology in frustrated hopping models*, Phys. Rev. B **78**(12), 125104 (2008), doi:[10.1103/PhysRevB.78.125104](https://doi.org/10.1103/PhysRevB.78.125104), [0803.3628](https://arxiv.org/abs/0803.3628).
- [67] A. Chubukov, *Pairing mechanism in fe-based superconductors*, Annual Review of Condensed Matter Physics **3**, 57 (2012), doi:[10.1146/annurev-conmatphys-020911-125055](https://doi.org/10.1146/annurev-conmatphys-020911-125055).
- [68] I. I. Mazin, D. J. Singh, M. D. Johannes and M. H. Du, *Unconventional Superconductivity with a Sign Reversal in the Order Parameter of LaFeAsO<sub>1-x</sub>F<sub>x</sub>*, Phys. Rev. Lett. **101**(5), 057003 (2008), doi:[10.1103/PhysRevLett.101.057003](https://doi.org/10.1103/PhysRevLett.101.057003).
- [69] T. Das and A. V. Balatsky, *Testing the sign-changing superconducting gap in iron-based superconductors with quasiparticle interference and neutron scattering*, Journal of Physics: Condensed Matter **24**, 182201 (2012), doi:[10.1088/0953-8984/24/18/182201](https://doi.org/10.1088/0953-8984/24/18/182201).
- [70] T. Das, J.-X. Zhu and M. J. Graf, *Theory of nodal  $s\pm$ -wave pairing symmetry in the pu-based 115 superconductor family*, Scientific Reports **5**, 8632 (2015), doi:[10.1038/srep08632](https://doi.org/10.1038/srep08632).
- [71] M. Tinkham, *Introduction to Superconductivity*, Dover Books on Physics Series. Dover Publications, ISBN 9780486134727 (2004).
- [72] M. Mandal, A. Kataria, C. Patra, D. Singh, P. K. Biswas, A. D. Hillier, T. Das and R. P. Singh, *Time-reversal symmetry breaking in frustrated superconductor Re<sub>2</sub>Hf*, Phys. Rev. B **105**(9), 094513 (2022), doi:[10.1103/PhysRevB.105.094513](https://doi.org/10.1103/PhysRevB.105.094513).
- [73] P. Neha, P. K. Biswas, T. Das and S. Patnaik, *Time-reversal symmetry breaking in topological superconductor sr<sub>0.1</sub>bi<sub>2</sub>se<sub>3</sub>*, Physical Review Materials **3**, 074201 (2019), doi:[10.1103/PhysRevMaterials.3.074201](https://doi.org/10.1103/PhysRevMaterials.3.074201).
- [74] A. Damle, L. Lin and L. Ying, *Compressed representation of kohn–sham orbitals via selected columns of the density matrix*, Journal of Chemical Theory and Computation **11**, 1463 (2015), doi:[10.1021/ct500985f](https://doi.org/10.1021/ct500985f).
- [75] A. Damle and L. Lin, *Disentanglement via entanglement: A unified method for wannier localization*, Multiscale Modeling & Simulation **16**, 1392 (2018), doi:[10.1137/17M1129696](https://doi.org/10.1137/17M1129696).

- [76] G. Pizzi, V. Vitale, R. Arita, S. Blügel, F. Freimuth, G. Géranton, M. Gibertini, D. Gresch, C. Johnson, T. Koretsune, J. Ibañez-Azpiroz, H. Lee *et al.*, *Wannier90 as a community code: new features and applications*, Journal of Physics: Condensed Matter **32**, 165902 (2020), doi:[10.1088/1361-648X/ab51ff](https://doi.org/10.1088/1361-648X/ab51ff).
- [77] P. Adhikary, S. Bandyopadhyay, T. Das, I. Dasgupta and T. Saha-Dasgupta, *Orbital-selective superconductivity in a two-band model of infinite-layer nickelates*, Physical Review B **102**, 1 (2020), doi:[10.1103/PhysRevB.102.100501](https://doi.org/10.1103/PhysRevB.102.100501).
- [78] T. Das and A. V. Balatsky, *Two energy scales in the magnetic resonance spectrum of electron and hole doped pnictide superconductors*, Physical Review Letters **106** (2011), doi:[10.1103/PhysRevLett.106.157004](https://doi.org/10.1103/PhysRevLett.106.157004).
- [79] G. Kresse and J. Furthmüller, *Efficient iterative schemes for ab initio total-energy calculations using a plane-wave basis set*, Phys. Rev. B **54**, 11169 (1996), doi:[10.1103/PhysRevB.54.11169](https://doi.org/10.1103/PhysRevB.54.11169).
- [80] G. Kresse and J. Furthmüller, *Efficiency of ab-initio total energy calculations for metals and semiconductors using a plane-wave basis set*, Comput. Mater. Sci. **6**(1), 15 (1996), doi:[https://doi.org/10.1016/0927-0256\(96\)00008-0](https://doi.org/10.1016/0927-0256(96)00008-0).
- [81] J. P. Perdew, K. Burke and M. Ernzerhof, *Generalized gradient approximation made simple*, Phys. Rev. Lett. **77**, 3865 (1996), doi:[10.1103/PhysRevLett.77.3865](https://doi.org/10.1103/PhysRevLett.77.3865).
- [82] P. E. Blöchl, *Projector augmented-wave method*, Phys. Rev. B **50**, 17953 (1994), doi:[10.1103/PhysRevB.50.17953](https://doi.org/10.1103/PhysRevB.50.17953).
- [83] G. Kresse and D. Joubert, *From ultrasoft pseudopotentials to the projector augmented-wave method*, Phys. Rev. B **59**, 1758 (1999), doi:[10.1103/PhysRevB.59.1758](https://doi.org/10.1103/PhysRevB.59.1758).
- [84] H. J. Monkhorst and J. D. Pack, *Special points for brillouin-zone integrations*, Phys. Rev. B **13**, 5188 (1976), doi:[10.1103/PhysRevB.13.5188](https://doi.org/10.1103/PhysRevB.13.5188).
- [85] S. L. Dudarev, G. A. Botton, S. Y. Savrasov, C. J. Humphreys and A. P. Sutton, *Electron-energy-loss spectra and the structural stability of nickel oxide: An lsd+u study*, Phys. Rev. B **57**, 1505 (1998), doi:[10.1103/PhysRevB.57.1505](https://doi.org/10.1103/PhysRevB.57.1505).
- [86] Y. Guo, Y. Zhao, S. Zhou and J. Zhao, *Oxidation behavior of layered Fe<sub>n</sub>GeTe<sub>2</sub> (n = 3, 4, 5) and Cr<sub>2</sub>Ge<sub>2</sub>Te<sub>6</sub> governed by interlayer coupling*, Nanoscale **14**(31), 11452 (2022), doi:[10.1039/D2NR02375J](https://doi.org/10.1039/D2NR02375J).
- [87] K. Momma and F. Izumi, *VESTA 3 for three-dimensional visualization of crystal, volumetric and morphology data*, J. Appl. Crystallogr. **44**(6), 1272 (2011), doi:[10.1107/S0021889811038970](https://doi.org/10.1107/S0021889811038970).
- [88] M. Winiarski and M. Samsel-Czekala, *The electronic structure of rare-earth iron silicide R<sub>2</sub>Fe<sub>3</sub>Si<sub>5</sub> superconductors*, Solid State Sci. **26**, 134 (2013), doi:[10.1016/j.solidstatesciences.2013.10.006](https://doi.org/10.1016/j.solidstatesciences.2013.10.006).
- [89] M. Samsel-Czekala and M. Winiarski, *Electronic structure and Fermi surface of iron-based superconductors R<sub>2</sub>Fe<sub>3</sub>Si<sub>5</sub> (R = Lu;Y;Sc) from first principles*, Intermetallics **31**, 186 (2012), doi:[10.1016/j.intermet.2012.07.003](https://doi.org/10.1016/j.intermet.2012.07.003).